12-23-1960

A Study of a Plane Dislocation Problem

Daniel D. Kana

A PLANE DISLO-CATION PROBLEM

KANA

A STUDY OF A
PLANE DISLOCATION PROBLEM

By

Daniel D. Kana

A Thesis

Submitted in Partial Fulfillment of the

Requirements for the Degree of

Master of Science in Mechanical Engineering

The University of New Mexico

1960

This thesis, directed and approved by the candidate's committee, has been accepted by the Graduate Committee of the University of New Mexico in partial fulfillment of the requirements for the degree of

MASTER OF SCIENCE

E. H. Castetter
Dean

December 23, 1960
Date

Thesis committee

Frederick D. Nelson
Chairman

R. C. Dove

Victor J. Hoglund

ABSTRACT

Elastic dislocation theory can be applied to plane problems involving discontinuous displacement in the plane domain. A particular problem of interest is a logarithmic spiral dislocation occurring in a thick-walled cylinder or at a hole in a large plate. This problem can closely simulate the stress condition resulting from Lueders' band formation in cylinders or plates. M. Stippes and F. D. Ju first extended elastic dislocation theory to problems involving doubly-connected, plane regions. The logarithmic spiral problem was first discussed in their work. Only a partial solution of the problem was considered.

This paper treats a more complete solution to the logarithmic spiral problem. Some changes in the basic dislocation theory are first accomplished to generalize the form of functions involved. The resulting equations are then applied to the logarithmic spiral dislocation at a hole in a large plate. A complete solution of pertinent stresses is obtained. Data are calculated to obtain the required dislocation relation along the logarithmic spiral cut, circumferential stress at the hole, and maximum shear stress along the dislocation cut.

An experimental solution of the same problem provided a possible method of confirming the validity of the analytical solution. The photoelastic technique was considered possible. However, before the actual experimental solution could be attempted, a model material and preparation procedure had to be determined. Of the several materials considered, adiprene plastic proved to be the best suited to the model preparation procedure determined to provide the proper dislocation stress result.

Photoelastic results from the experimental solution confirmed very well the results of the analytical solution. Compared stresses agreed very well with the analytical predictions. Although no great effort was exerted to control the experimental dislocation relation, it too, closely approximated that required by the analytical solution. The most pronounced discrepancy between the two solutions resulted in the stress pattern on the upper side of the dislocation cut. An apparent explanation is the lack of controlled absolute displacement as well as an adequately controlled dislocation relation along the cut.

The immediate results of this work were the confirmation of the analytical method of approach to the dislocation problem, and an indication of a good experimental method of further studying this type of problem. In addition, there is an indication of a discrepancy in the Volterra dislocation theory as a result of this work. Some refinements in the experimental method are suggested. Problems having simpler geometrical dislocation shapes could be solved even more easily than the logarithmic spiral problem using the experimental procedure that resulted from this work.

CONTENTS

Page

LIST OF TABLES

LIST OF ILLUSTRATIONS

Drawings and Photographs

Curves

NOTATIONS

σ	Normal stress
τ	Shearing stress
σ_x , σ_y , τ_{xy}	Stress components in Cartesian coordinates
σ_r , σ_θ , $\tau_{r\theta}$	Stress components in polar coordinates
σ_n , τ_n	Stress components on the plane normal to the dislocation cut
u_x , u_y	Displacement components in Cartesian coordinates
u_n , u_t	Displacement components normal and tangent respectively to the dislocation curve
$U(z, \bar{z})$	Airy stress function
$\phi_1(z)$, $\phi_2(z)$	Functions of z in the Airy stress function
λ , μ	Lame's constants, the latter is identified as the modulus of rigidity
δ	Constant, the dislocation of the cut at the inner boundary
σ' , τ'	Stress discontinuity along the cut
$u' = u^+ - u^-$	Dislocation, or displacement discontinuity along the cut
ν	Poisson's ratio
κ	Constant, $\frac{3-\nu}{1+\nu}$ in plane stress and $3-4\nu$ in plane strain case
α	Angle between x-axis and tangent to cut
$z_o = x_o + iy_o$	An arbitrary point on the cut
$\mathcal{R}e$	Indicating the real part of a function
$\mathcal{I}m$	Indicating the imaginary part of a function

I. INTRODUCTION

Preliminary

The use of the elastic dislocation concept is a comparatively new approach to the solution of plane stress problems with discontinuous displacement in the plane domain. A particular problem to which this approach can be applied is a logarithmic spiral dislocation cut in a doubly-connected plane circular region. This is a practical problem, for it closely approximates the actual problem of Lueders' band formation in the cross sectional plane in thick-walled cylinders subjected to high internal pressure. A close approximation to the problem will result if the logarithmic spiral constant angle β is 45° (Figure 1). The logarithmic spiral dislocation can be described as a logarithmic spiral plane curve along which displacements are discontinuous. The curve extends from the inner boundary of the doubly-connected region and terminates within the region. The dislocation causes stress in the region. Elastic dislocation theory allows for some of the stress components to be discontinuous along the dislocation cut. Stresses and displacements are continuous everywhere in the region except along the dislocation cut so that plane elastic theory is applicable. Along the cut in the plane region only the normal and shear stress components on the tangent to the cut must be continuous so that Newton's third law will be satisfied.

Elastic Dislocation Theory

Mann's work (4) covered elastic dislocations in a simply-connected region, while Stippes and Ju (6), and Ju (1), extended the theory

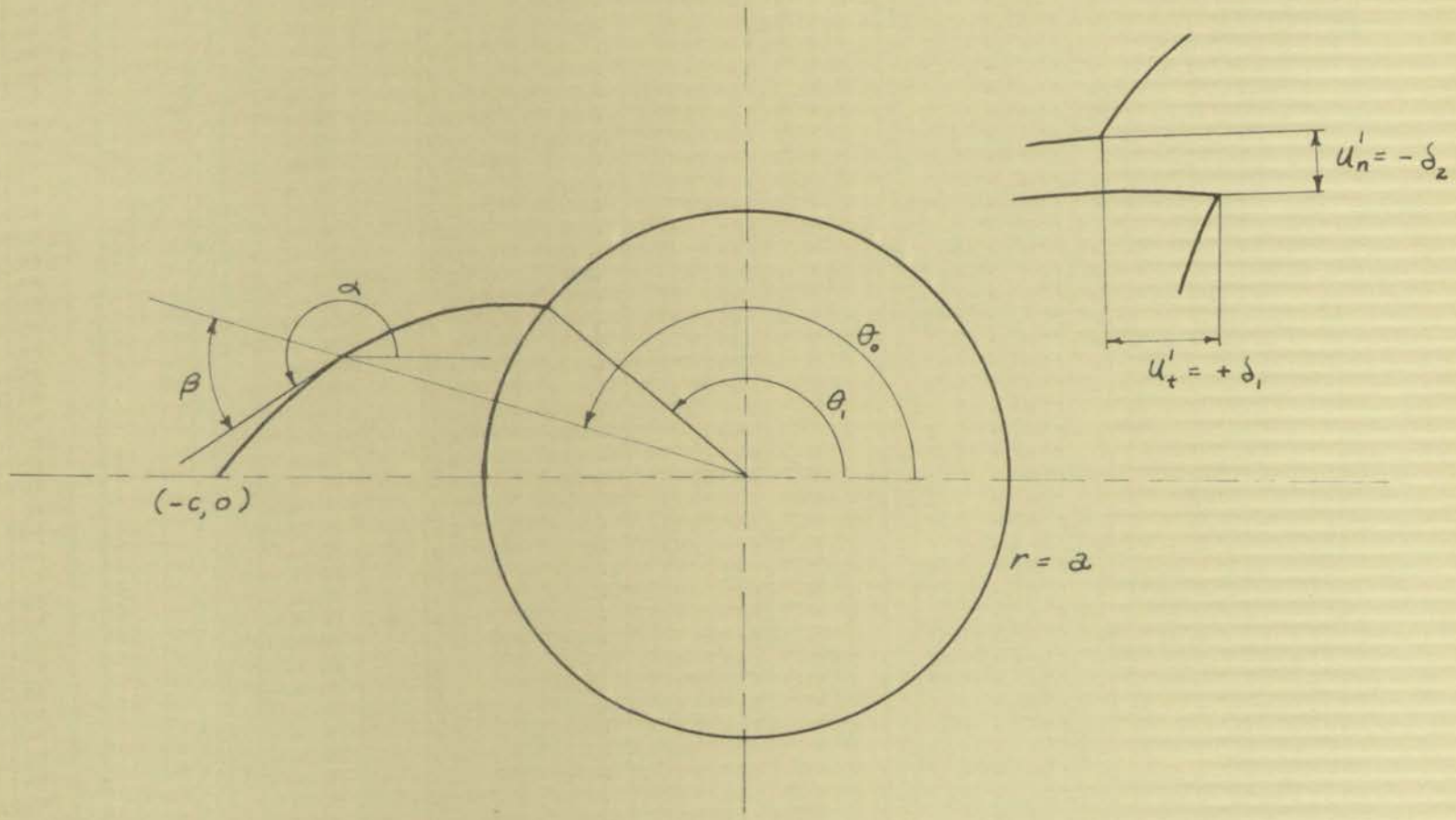

Figure 1

to multiply-connected regions. The latter two works provide the entire background for this paper. Accordingly, the following is a brief summary of these works. Several applied problems were discussed in these works, but only the logarithmic spiral dislocation is the best approximation to the Lueders' band problem.

A plane circular, doubly-connected region is convenienctly expressed in the complex variable representation. For the plane problem the biharmonic equation for the Airy stress function $U(z, \bar{z})$

$$\nabla^4 U = 0$$

is expressed as

$$\frac{\partial^4 U}{\partial z^2 \partial \bar{z}^2} = 0$$

where

$$z = x + iy \quad \text{and} \quad \bar{z} = x - iy$$

the most general solution of this equation is

$$2U = \bar{z}\,\Phi_1(z) + z\,\bar{\Phi}_1(\bar{z}) + \Phi_2(z) + \bar{\Phi}_2(\bar{z})$$

Based on the plane elastic theory, the relation between the displacement and stress components and the functions $\Phi_1(z)$ and $\Phi_2(z)$ are as follows:

$$2\mu(u_x + iu_y) = \kappa\Phi_1(z) - z\,\bar{\Phi}_1'(\bar{z}) - \bar{\Phi}_2'(\bar{z})$$

$$\sigma_x + \sigma_y = 2\left[\Phi_1'(z) + \bar{\Phi}_1'(\bar{z})\right]$$

$$\sigma_y - \sigma_x + 2i\tau_{xy} = 2\left[\bar{z}\,\Phi_1''(z) + \Phi_2''(z)\right]$$

These equations, when expressed in terms of the normal and tangential components along the cut, as well as polar components, become

$$
\begin{aligned}
2\mu(u_t + iu_n)e^{i\alpha} &= \kappa\phi_1(z) - z\overline{\phi}_1'(\bar{z}) - \overline{\phi}_2'(\bar{z}) \\
\sigma_n + i\tau_n &= \phi_1'(z) + \overline{\phi}_1'(\bar{z}) + \left[\bar{z}\phi_1''(z) + \phi_2''(z)\right]e^{2i\alpha} \\
\sigma_r - i\tau_{r\theta} &= \phi_1'(z) + \overline{\phi}_1'(\bar{z}) - \left[\bar{z}\phi_1''(z) + \phi_2''(z)\right]e^{2i\theta}
\end{aligned}
\tag{1}
$$

Figure 2 may be helpful in relating the cartesian coordinates with normal and tangential coordinates.

The basic assumptions used are

$$
\left.
\begin{aligned}
u_t' &= u_t^+ - u_t^- = 0 \\
u_n' &= u_n^+ - u_n^- = 0
\end{aligned}
\right\}
\quad \text{at the terminus } (-c,\ 0) \tag{2}
$$

$$
\left.
\begin{aligned}
u_t' &= \delta_1 \\
u_n' &= \delta_2
\end{aligned}
\right\}
\quad \begin{array}{l}\text{at the inner boundary} \\ \text{end } (a\cos\theta_1,\ a\sin\theta_1)\end{array} \tag{3}
$$

$$
\left.
\begin{aligned}
\sigma_n' &= \sigma_n^+ - \sigma_n^- = 0 \\
\tau_n' &= \tau_n^+ - \tau_n^- = 0
\end{aligned}
\right\}
\quad \begin{array}{l}\text{Newton's third law} \\ \text{along the cut}\end{array} \tag{4}
$$

A traction free case is assumed for simplicity. Hence, the boundary conditions are

$$
\sigma_r = \tau_{r\theta} = 0 \tag{5}
$$

at both the inner and outer boundaries. The functions $\phi_1(z)$ and $\phi_2(z)$ are composed of multiple-valued parts and single-valued parts.

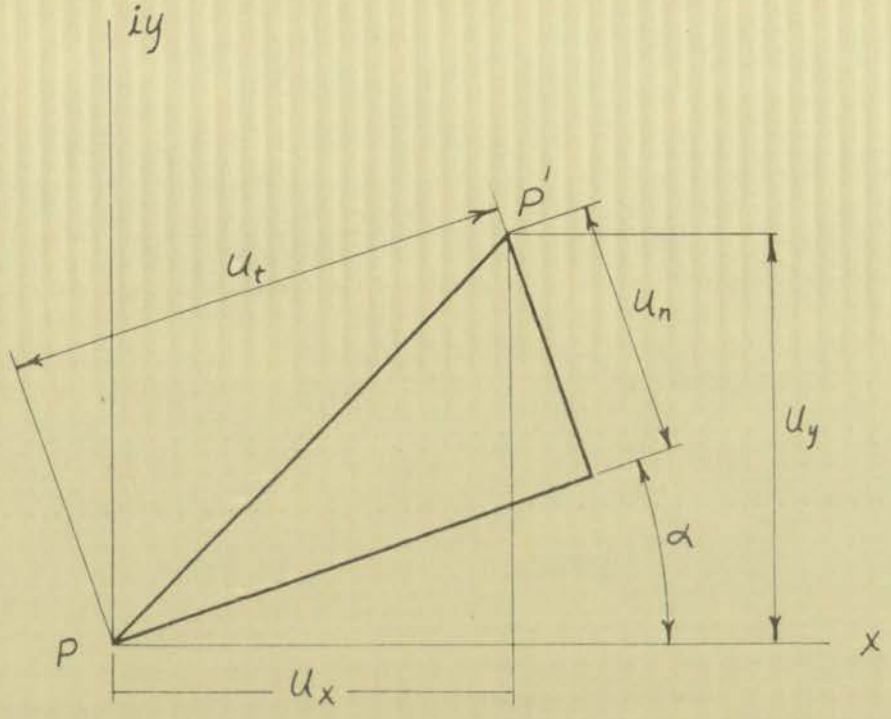
iy
P'
u_t
u_n
u_y
α
P
x
u_x

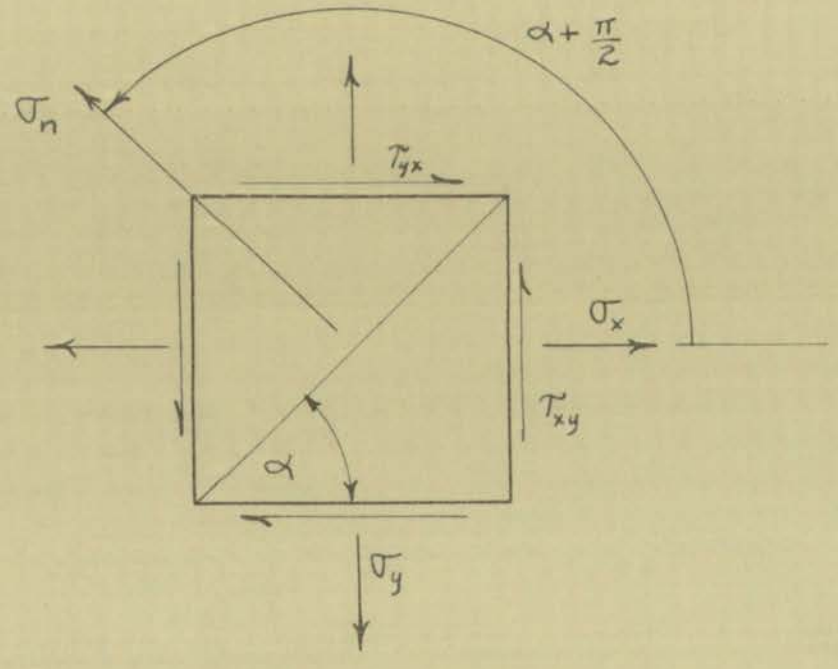
$\alpha + \frac{\pi}{2}$
σ_n
τ_{yx}
σ_x
τ_{xy}
α
σ_y

Figure 2

The multiple-valued part is expressed as a logarithmic form. The functions are

$$\Phi_1(z) = A(z) \ln \frac{z+c}{z} + C(z)$$
$$\Phi_2(z) = B(z) \ln \frac{z+c}{z} + D(z) \qquad (6)$$

where A(z), B(z), C(z), and D'(z) are all analytic. Furthermore, at the terminus

$$A(-c, 0) = B(-c, 0) = 0 \qquad (7)$$

so that the functions remain finite at this point.

The equations (1) are manipulated to result in terms of dislocation components to facilitate determination of multiple-valued terms, since only multiple-valued terms are affected by conditions along the cut. This results in the two basic equations

$$2\mu(u_t' + i u_n') e^{i\alpha} = -2\pi i \left[\kappa A(z_0) + z_0 \overline{A}'(\overline{z}_0) + \overline{B}'(\overline{z}_0)\right] \qquad (8)$$

$$A'(z_0) - \overline{A}'(\overline{z}_0) + \left[\overline{z}_0 A''(z_0) + B''(z_0)\right] e^{2i\alpha} = 0 \qquad (9)$$

The z_0 indicate values along the cut only.

The analytic functions A(z) and B(z) in (6) above, are expanded into the Laurent series forms:

$$A(z) = \sum_{-\infty}^{\infty} (R_n + i S_n) z^n$$
$$B(z) = \sum_{-\infty}^{\infty} (P_m + i Q_m) z^m \qquad (10)$$

These functions, when substituted into (8) and (9) along with the previous given assumptions, have their constants determined. A substitution into the last of equations (1) allows the multiple-valued part of the stress to be expressed in polar, then in trigonometric series form,

a form in which the single-valued parts can readily be expressed. The single-valued terms are determined by first expressing the functions C(z) and D'(z) in the Laurent series form also.

$$C(z) = \sum_{-\infty}^{\infty} (K_n + i L_n) z^{n+1}$$
$$D'(z) = \sum_{-\infty}^{\infty} (M_n + i N_n) z^{n-1} \qquad (11)$$

D'(z) only need be specified and not D(z) since this function appears in the basic equations in the first derivitive as the lowest order. These functions are substituted into the last of equations (1) and expressed in polar form, then trigonometric form. Both the multiple-valued and single-valued parts of the stresses then result in trigonometric infinite series, but only the single-valued part constants are undetermined. The application of the boundary conditions of a specified problem then allows the equating of coefficients of like terms to determine the single-valued constants.

The method is applied to several shapes of dislocations in a doubly-connected region. One of them is the logarithmic spiral where the dislocation curve is

$$\theta_o = \pi + \tan\beta \ln \frac{r_o}{c} \qquad (12)$$

and the angle α is

$$\alpha = \theta_o + \beta \qquad (13)$$

In reference (1) the specific problems are developed to where the constants are all determined. However, analytical expressions for stresses are not given for any of the problems to which the theory is applied.

Restriction of Solution

Before making a further study of the preceding theory and logarithmic spiral application it is expedient to show that a restriction of solution exists once certain conditions are chosen. Equations (8) and (9) express the two basic relations governing the analytic functions A(z) and B(z) that appear in the $\ln \frac{z+c}{z}$ terms of the functions (6).

$$2\mu(u_t' + i u_n')e^{i\alpha} = -2\pi i\left[\kappa A(z_0) + z_0 \bar{A}'(\bar{z}_0) + \bar{B}'(\bar{z}_0)\right] \tag{8}$$

$$A'(z_0) - \bar{A}'(\bar{z}_0) + \left[\bar{z}_0 A''(z_0) + B''(z_0)\right]e^{2i\alpha} = 0 \tag{9}$$

It must be recalled that both these equations are based on the $\ln \frac{z+c}{z}$ form as the multiple-valued part of the functions $\phi_1(z)$ and $\phi_2(z)$. Equation (8) relates the dislocation relation to these functions, while equation (9) expresses them under the conditions (4), Newton's third law. Therefore, any functions A(z) and B(z) that satisfy (9) may then be substituted into (8) to see what dislocation relation they allow for a given shape of cut. Specifically the logarithmic spiral cut has the relation

$$\alpha = \beta + \theta_0$$

where β = constant. It will be shown that once the logarithmic spiral shape is chosen, only one solution to equation (9) is possible.

The forms (10) of A(z) and B(z) are substituted into equation (9) to get

$$\sum_{-\infty}^{\infty}\Big\{n(R_n+iS_n)z_o^{n-1}-n(R_n-iS_n)\bar{z}_o^{n-1}+n(n-1)(R_n+iS_n)e^{2i\beta}z_o^{n-1}$$
$$+m(m-1)(P_m+iQ_m)e^{2i(\beta+\theta_o)}z_o^{m-2}\Big\}=0$$

or using a trigonometric identify and regrouping

$$\sum_{-\infty}^{\infty}\Big\{\Big\{\Big[nR_n+n(n-1)(R_n\cos 2\beta-S_n\sin 2\beta)\Big]$$
$$+i\Big[nS_n+n(n-1)(R_n\sin 2\beta+S_n\cos 2\beta\Big]\Big\}z_o^{n-1}$$
$$-\Big[n(R_n-iS_n)\Big]\bar{z}_o^{n-1}+m(m-1)\Big\{\Big[P_m\cos 2(\beta+\theta_o)-Q_m\sin 2(\beta+\theta_o)\Big]$$
$$+i\Big[P_m\sin 2(\beta+\theta_o)+Q_m\cos 2(\beta+\theta_o)\Big]\Big\}z_o^{m-2}\Big\}=0$$

Any values of m and n that together satisfy the above equation provide a solution. Recall that β = constant for the logarithmic spiral case. The most obvious choice of m and n is

$$m = 0, \quad n = 0$$

which makes all coefficients zero. Further selections are somewhat more complicated. The points z_o^{+n-1} and $\bar{z}_o^{+n-1}$ are always distinctly different points except at (-c, 0). However, for m = n+1, z_o^{m-2} and z_o^{n-1} become the same point. In order for the equation to hold, the coefficients of any like terms must sum to zero, and coefficients of any single unlike terms must vanish individually. In view of this,

another possible combination is

$$m = 1, \quad n = 1 \qquad \text{to give}$$

$$R_1 + iS_1 - R_1 + iS_1 = 0$$

which is true if $S_1 = 0$. Any attempt at using $m = n+1$ results in

$$\left[nR_n + n(n-1)(R_n\cos 2\beta - S_n \sin 2\beta)\right] + (n+1)n\left[P_m \cos 2(\beta+\theta_o) - Q_m \sin 2(\beta+\theta_o)\right] + i\left\{\left[nS_n + n(n-1)(R_n \sin 2\beta + S_n \cos 2\beta)\right] + (n+1)n\left[P_m \sin 2(\beta+\theta_o) + Q_m \cos 2(\beta+\theta_o)\right]\right\}$$

as the coefficient of the z_o^{n-1} term. This coefficient can vanish only if $n = 0$, which is the same as $n = 0$, $m = 1$, the same values found earlier. No other values of m and n are possible. As a result, the forms of the functions A(z) and B(z), based on the conditions given are

$$A(z) = R_1 z + (R_o + iS_o)$$

$$B(z) = (P_1 + iQ_1)z + (P_o + iQ_o) \qquad (14)$$

These are the only possible forms that will satisfy equation (9) when the logarithmic spiral dislocation cut is used, therefore, the solution is unique for that case. Since by equation (8) these forms determine the dislocation relation, it also is unique for this case. These are the forms originally used in references (1) and (6).

Extent of Problem

This work is an extension of the work in references (1) and (6). The basic theory will be further studied by changing some of the basic assumptions and determining the results for the case of the logarithmic spiral cut. A complete analytical solution of the logarithmic spiral cut extending from a hole in a large plate will be attained, including series form expressions for stresses at pertinent locations in the region. This will allow tabulation of data so that stress curves can be plotted. As in the reference works summarized, only one cut in a given region will be considered with the understanding that superposition would allow any number of cuts in a region as long as the cuts do not cross.

An experimental study will then be conducted to try to correlate experimental results with the analytical results. The photoelastic technique will be employed. Various preliminary studies must be conducted before the actual problem solution is attempted, however. Specifically, a suitable model material and model preparation techniques have to be determined. For this solution no particular controlled dislocation relation along the cut is specified, however, a somewhat approximation to that determined from the analytical solution will be attempted. The correlation of experimental and analytical results will then be from a position of a comparison of shape of stress patterns rather than a comparison of absolute stress magnitudes. Only relative stress magnitudes will be considered.

II. STUDY OF ALTERED FUNCTIONS AND ASSUMPTIONS

It is desirable to make a study of altering the functions of the dislocation theory summarized in Chapter I. Such a study could result in the improvement of the forms of the functions $\Phi_1(z)$ and $\Phi_2(z)$. In particular, the function $\Phi_2(z)$ can readily be altered to a somewhat more general form. When this is attempted, however, difficulty can arise in using the condition (7) which was imposed to prevent infinite displacements at the terminus (-c, 0). This difficulty causes condition (2) to be violated, thereby not allowing a possible physical solution. An alternate procedure is to alter the form of $\Phi_2(z)$, do not specify the conditions (2) and (7), and use the more general assumption that all displacements must remain finite. The following development and resulting solution is based on these changes in functions and assumptions.

Conditions and Assumptions

Equations (1) will hold:

$$
\begin{aligned}
2\mu(u_t + iu_n)e^{i\alpha} &= \kappa\Phi_1(z) - z\overline{\Phi}_1'(\bar{z}) - \overline{\Phi}_2'(\bar{z}) \\
\sigma_n + i\tau_n &= \Phi_1'(z) + \overline{\Phi}_1'(\bar{z}) + \left[\bar{z}\Phi_1''(z) + \Phi_2''(z)\right]e^{2i\alpha} \qquad (1) \\
\sigma_r - i\tau_{r\theta} &= \Phi_1'(z) + \overline{\Phi}_1'(\bar{z}) - \left[\bar{z}\Phi_1''(z) + \Phi_2''(z)\right]e^{2i\theta}
\end{aligned}
$$

The following assumptions are specified:

$$\left.\begin{aligned} u_t' &= \delta_1 \\ u_n' &= \delta_2 \end{aligned}\right\} \quad \text{at the inner boundary end } (a\cos\theta_1,\ a\sin\theta_1) \tag{3}$$

$$\left.\begin{aligned} \sigma_n' &= \sigma_n^+ - \sigma_n^- = 0 \\ \tau_n' &= \tau_n^+ - \tau_n^- = 0 \end{aligned}\right\} \quad \text{Newton's third law along the cut} \tag{4}$$

$$\sigma_r = \tau_{r\theta} = 0 \qquad \text{along the boundaries} \tag{5}$$

$$\begin{aligned} \Phi_1(z) &= A(z)\ln\frac{z+c}{z} + C(z) \\ \Phi_2'(z) &= B(z)\ln\frac{z+c}{z} + D(z) \end{aligned} \tag{15}$$

where A(z), B(z), C(z), and D(z) are all analytic in the region. Also

All displacements must remain finite.

Note that $\Phi_2'(z)$ has been specified in place of $\Phi_2(z)$. Since only the derivitive $\Phi_2'(z)$ appears in the equations (1) as the lowest order of that function, it is necessary only to find the form of the derivitive rather than the function itself, as was done in references (1) and (6).

Basic Equations

A development similar to that used previously is utilized. Using the first of equations (1) for along the cut there results:

$$2\mu(u_t' + iu_n')e^{i\alpha} = 2\mu e^{i\alpha}\left[(u_t+iu_n)^+ - (u_t+iu_n)^-\right]$$

$$= \left\{\kappa A(z)\ln\frac{z_o+c}{z_o} - z_o\left[\bar{A}'(\bar{z}_o)\ln\frac{\bar{z}_o+c}{\bar{z}_o}\right] - \bar{B}(\bar{z}_o)\ln\frac{\bar{z}_o+c}{\bar{z}_o}\right\}^+$$

$$-\left\{\kappa A(z_o)\ln\frac{z_o+c}{z_o} - z_o\left[\bar{A}'(\bar{z}_o)\ln\frac{\bar{z}_o+c}{\bar{z}_o}\right] - \bar{B}(\bar{z}_o)\ln\frac{\bar{z}_o+c}{\bar{z}_o}\right\}^-$$

All non-logarithmic terms dropped out. In Figure 1, with the top side of the cut designated + and the bottom designated - , the following results:

$$\left(\ln \frac{z_o+c}{z_o}\right)^+ - \left(\ln \frac{z_o+c}{z_o}\right)^- = -2\pi i$$
$$\left(\ln \frac{\bar{z}_o+c}{\bar{z}_o}\right)^+ - \left(\ln \frac{\bar{z}_o+c}{\bar{z}_o}\right)^- = +2\pi i \qquad (16)$$

These can be shown easily by using the relations

$$\ln z^+ = \ln|z| + i\theta$$
$$\ln z^- = \ln|z| + i(\theta - 2\pi)$$

When equations (16) are substituted into the remaining part of the dislocation relation there results

$$2\mu(u_t' + iu_n')e^{i\alpha} = -2\pi i\left[\kappa A(z_o) + z_o\bar{A}'(\bar{z}_o) + \bar{B}(\bar{z}_o)\right] \qquad (17)$$

It will be noted that there is a slight difference from equation (8). Now by substituting equations (15) and (16) into the second of equations (1), and using conditions (4) there results:

$$A'(z_o) - \bar{A}'(\bar{z}_o) + \left[\bar{z}_o A''(z_o) + B'(z_o)\right]e^{2i\alpha} = 0 \qquad (18)$$

It will be noted that there is a slight difference from equation (9).

Application to Logarithmic Spiral

The question that now arises is whether a further solution is possible using the new equations (17) and (18) for a specific shape of

dislocation such as the logarithmic spiral. A development similar to that of Chapter I is first utilized. The Laurent series forms of the functions A(z) and B(z) are

$$A(z) = \sum_{-\infty}^{\infty} (R_n + i S_n) z^n$$
$$B(z) = \sum_{-\infty}^{\infty} (P_m + i Q_m) z^m \qquad (10)$$

Together with equation (18) these series give

$$\sum_{-\infty}^{\infty} \Big\{ n(R_n + iS_n) z_o^{n-1} - n(R_n - iS_n) \bar{z}_o^{n-1} + n(n-1)(R_n - iS_n) e^{2i\beta} z_o^{n-1} + m(P_m + iQ_m) e^{2i(\beta+\theta_o)} z_o^{m-1} \Big\} = 0$$

As was indicated in Chapter I, the coefficients of the like terms must vanish. Recall also that β is constant for the logarithmic spiral case. The possible values of m and n are

$m = 0, \quad n = 0, \ 1$ only, giving further

$$S_1 = 0.$$

The forms of the functions A(z) and B(z) must be

$$A(z) = R_1 z + R_o + i S_o$$
$$B(z) = P_o + i Q_o \qquad (19)$$

It is now necessary to use the condition that displacements remain finite. Equations (15) are substituted into the first of equations (1). The only critical point is (-c, 0). It is required that

$$\lim_{z \to (-c,0)} \left[\kappa \Phi_1(z) - z \bar{\Phi}_1'(\bar{z}) - \bar{\Phi}_2'(\bar{z}) \right] e^{i\alpha} = \text{finite}$$

At (-c, 0), $e^{i\alpha}$ becomes $e^{-i\beta}(1 - 0)$ = constant, therefore, the bracketed term is the only affected part:

$$\lim_{z\to(-c,0)} \left\{ K A(z) \ln \frac{z+c}{z} + K C(z) - z \left[\bar{A}'(\bar{z}) \ln \frac{\bar{z}+c}{\bar{z}} - \bar{A}(\bar{z}) \left(\frac{1}{\bar{z}+c} - \frac{1}{\bar{z}} \right) + \bar{C}'(\bar{z}) \right] - \bar{B}(\bar{z}) \ln \frac{\bar{z}+c}{\bar{z}} - \bar{D}(\bar{z}) \right\} = \text{finite}$$

The 1/z and $1/\bar{z}$ terms can be dropped since z = 0 is not in the region of concern. The C(z), $\bar{C}'(z)$, and $\bar{D}(\bar{z})$ terms can be dropped since they are functions of powers of z in Laurent series form, and will not become infinite in the region. There remains

$$\lim_{z\to(-c,0)} \left\{ K A(z) \ln(z+c) - \left[z \bar{A}'(\bar{z}) + \bar{B}(\bar{z}) \right] \ln(\bar{z}+c) + z \bar{A}(\bar{z}) \left(\frac{1}{\bar{z}+c} \right) \right\} = \text{finite}$$

The only way this can occur is for the like coefficients to vanish.

$$\lim_{z\to(-c,0)} z \bar{A}(\bar{z}) = 0 \quad \text{indicates that}$$

$$\bar{A}(-c, 0) = 0$$

This will also allow the vanishing of the first term of the equation. Using this with equations (19), there results

$$R_0 = R_{1c} \ , \ S_0 = 0.$$

For the second term of the above equation:

$$\lim_{z\to(-c,0)} \left[z \bar{A}'(\bar{z}) + \bar{B}(\bar{z}) \right] = 0$$

Putting equations (19) into this, there results

$$P_o = R_1 c \quad , \quad Q_o = 0.$$

The final form of equations (20) is

$$A(z) = R_1 (z + c)$$
$$B(z) = R_1 c. \tag{20}$$

Dislocation Relations

To find the dislocation forms, equations (20) above are substituted into equation (17). Upon rearrangement

$$u_t' + i u_n' = -\frac{\pi R_1}{\mu}(K+1) i \left[r_o e^{i\theta_o} + C \right] e^{-i\alpha}$$

Using the trigonometric form of z, along with $\alpha = \beta + \theta_o$, and solving for real and imaginary parts gives:

$$u_t' = -\pi R_1 \frac{(K+1)}{\mu} \left[r_o \sin\beta + C \sin\alpha \right]$$

$$u_n' = -\pi R_1 \frac{(K+1)}{\mu} \left[r_o \cos\beta + C \cos\alpha \right]$$

It can be seen from these equations that the requirement of finite displacements automatically satisfies the condition for a practical problem:

$$u_t' = u_n' = 0 \quad \text{at} \quad (-c, 0),$$

even though it was not specified and used mathematically. Using trigonometric relations and the equation of the logarithmic spiral:

$$\theta_o = \pi + \tan\beta \ln \frac{r_o}{C}$$

there results

$$u_t' = -\pi R_1 \frac{(K+1)}{\mu}\left[r_o \sin\beta - C \sin\left(\beta + \tan\beta \ln \frac{r_o}{C}\right)\right]$$

$$u_n' = -\pi R_1 \frac{(K+1)}{\mu}\left[r_o \cos\beta - C \cos\left(\beta + \tan\beta \ln \frac{r_o}{C}\right)\right]$$

Two equations for one unknown indicates that one equation is dependent, or using conditions (3), that δ_1 and δ_2 are related. Choosing one is sufficient. At the inner boundary $r_o = a$, choosing δ_2 as independent gives

$$R_1 = -\frac{\delta_2 \mu}{\pi(K+1)}\left[\frac{1}{a\cos\beta - C\cos\left(\beta + \tan\beta \ln \frac{a}{C}\right)}\right] \qquad (21)$$

Substituting this into the above equations gives

$$u_t' = \delta_2 \frac{r_o \sin\beta - C \sin(\beta + \tan\beta \ln r_o/C)}{a\cos\beta - C\cos(\beta + \tan\beta \ln a/C)}$$

$$u_n' = \delta_2 \frac{r_o \cos\beta - C \cos(\beta + \tan\beta \ln r_o/C)}{a\cos\beta - C\cos(\beta + \tan\beta \ln a/C)} \qquad (22)$$

and combining the two gives

$$\delta_1 = \delta_2 \frac{a\sin\beta - C\sin(\beta + \tan\beta \ln a/C)}{a\cos\beta - C\cos(\beta + \tan\beta \ln a/C)} \qquad (23)$$

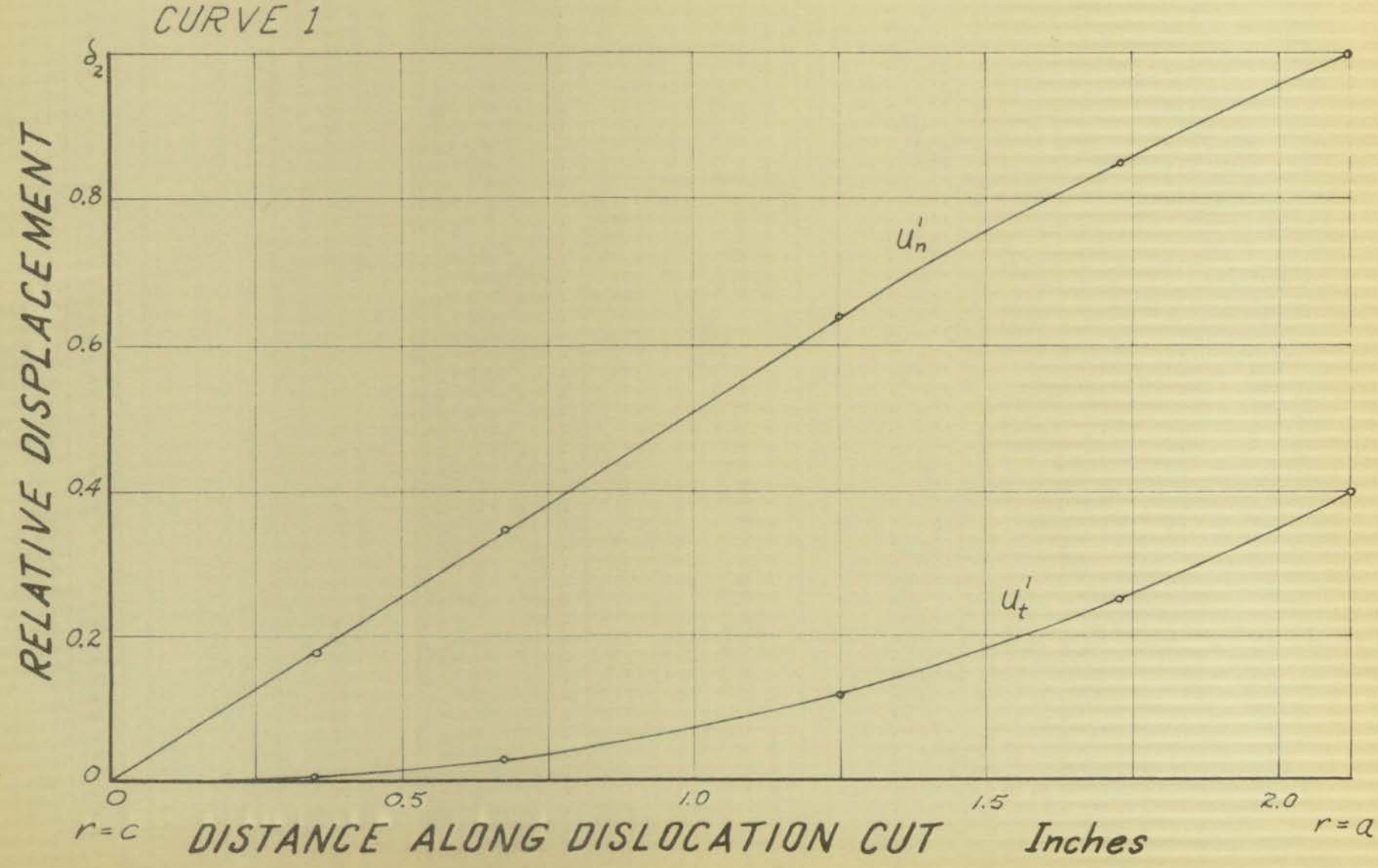
CURVE 1
RELATIVE DISPLACEMENT
δ_2
0.8
0.6
0.4
0.2
0
u_n'
u_t'
0
0.5
1.0
1.5
2.0
r=c
DISTANCE ALONG DISLOCATION CUT
Inches
r=a

These equations are identical to the results obtained for the logarithmic spiral case in references (1) and (6). A plot of the equations (22) against r_o for $\beta = 45^o$ is shown on Curve 1. As indicated in the above references and illustrated in Figure 2,

$+ \delta_z$ means interference of material,

$- \delta_z$ means a separation of material.

It can be seen from the above mentioned plot that u_n' is very nearly linear along the dislocation cut.

Expansion of Single-valued Terms

The single-valued terms C(z) and D(z) of equations (15) are next to be manipulated into a trigonometric series form. These functions can be expressed in Laurent series:

$$C(z) = \sum_{-\infty}^{\infty} (K_n + iL_n) z^{n+1}$$
$$D(z) = \sum_{-\infty}^{\infty} (M_n + iN_n) z^{n-1} \qquad (24)$$

The difference in powers is for mathematical convenience. To obtain the trigonometric series for the single-valued part of the stresses, the above Laurent series are substituted into the third of equations (1). In addition, the polar form of z is used, the limits are changed, and the functions are grouped to give for the single-valued part of the stresses

$$(\sigma_r - i\tau_{r\theta})_{SV} = 2K_o + \frac{M_o}{r^2} + \left(2rK_1 + \frac{2}{r^3}M_{-1}\right)\cos\theta$$
$$+ \sum_{2}^{\infty} \Big[-(n-2)(n+1) r^n K_n - (n-1)(n+2) r^{-n} K_{-n}$$
$$- (n-1) r^{n-2} M_n + (n+1) r^{-(n+2)} M_{-n} \Big] \cos n\theta \qquad (25)$$

$$+(-2rL_1+2r^{-3}N_{-1})\sin\theta$$

$$+\sum_2^\infty\Big[(n+1)(n-2)r^nL_n-(n-1)(n+2)r^{-n}L_{-n}$$

$$+(n-1)r^{n-2}N_n+(n+1)r^{-(n+2)}N_{-n}\Big]\sin n\theta$$

$$+i\Big\{\frac{N_0}{r^2}+(-2rL_1+2r^{-3}N_{-1})\cos\theta+\sum_2^\infty\Big[-n(n+1)r^nL_n$$

$$-n(n-1)r^{-n}L_{-n}-(n-1)r^{n-2}N_n+(n+1)r^{-(n+2)}N_{-n}\Big]\cos n\theta$$

$$+(-2rK_1-2r^{-3}M_{-1})\sin\theta+\sum_2^\infty\Big[-n(n+1)r^nK_n$$

$$+n(n-1)r^{-n}K_{-n}-(n-1)r^{n-2}M_n-(n+1)r^{-(n+2)}M_{-n}\Big]\sin n\theta\Big\}$$

Equation (25) is exactly the same as equation (17) of reference (1). The equations are identical since the form of D(z) in equations (24) is the same as that chosen for D'(z) in reference (1). Note that equation (25) is independent of the shape of the dislocation cut.

Expansion of Multiple-valued Terms

The single-valued part of the stress is now in the trigonometric series form with undetermined coefficients. The coefficients are determined by expanding the multiple-valued part of the stress into trigonometric series and applying the condition

$$\sigma_r=\tau_{r\theta}=0 \qquad \text{on the boundaries.} \qquad (5)$$

This procedure is possible since the multiple-valued part of the stress is already completely determined independent of the geometrical shape of the region, for it depends only on the already determined functions A(z) and B(z). In addition

$$\sigma_r - i\tau_{r\theta} = (\sigma_r - i\tau_{r\theta})_{sv} + (\sigma_r - i\tau_{r\theta})_{mv} \tag{26}$$

indicates that like coefficients of the two summed series must vanish to satisfy condition (5).

To obtain the preliminary expressions for the multiple-valued part of the stress, equations (20) are substituted into equations (15), and these into the third of equations (1). There results for the multiple-valued part only:

$$(\sigma_r - i\tau_{r\theta})_{mv} = 2\mathcal{R}e\left\{R_1\left[\ln\frac{z+c}{z} - \frac{c}{z}\right]\right\} - R_1 c^2\left[\frac{1 - e^{2i\theta}}{z(z+c)}\right] \tag{27}$$

The functions on the right side of the equation are those that must be expanded into trigonometric series forms. How the expansion is accomplished depends on the function. It will be noted that the boundaries are at

$$|z| < c \quad \text{and} \quad |z| > c$$

$$\text{or} \quad r < c \quad \text{and} \quad r > c \,,$$

therefore, a separate expansion of each function for each case is necessary. Appendix II gives the mathematical details of the expansions. These expansions substituted into equation (27) give:

For $|z| < c$

$$(\sigma_r - i\tau_{r\theta})_{mv} = R_1\left\{\sum_2^\infty \left[\frac{2(-1)^{n+1}}{n} + (-1)^n\left(1-\frac{c^2}{r^2}\right)\right]\left(\frac{r}{c}\right)^n \cos n\theta + 2\ln\frac{c}{r}\right.$$
$$\left. + \left(\frac{r}{c} - \frac{2c}{r}\right)\cos\theta + 1 + i\left\{\left(1-\frac{c^2}{r^2}\right)\sum_2^\infty \left[(-1)^n\left(\frac{r}{c}\right)^n \sin n\theta\right] + \left(\frac{2c}{r} - \frac{r}{c}\right)\sin\theta\right. \tag{28}$$

For $|z| > c$

$$(\sigma_r - i\tau_{r\theta})_{mv} = R_1\left\{\frac{c^2}{r^2} - \frac{c^3}{r^3}\cos\theta + \sum_2^\infty \left[\frac{2(-1)^{n+1}}{n} + (-1)^n\left(\frac{c^2}{r^2}-1\right)\right]\left(\frac{c}{r}\right)^n \cos n\theta\right.$$
$$\left. + i\left[\frac{c^3}{r^3}\sin\theta + \left(1-\frac{c^2}{r^2}\right)\sum_2^\infty (-1)^n\left(\frac{c}{r}\right)^n \sin n\theta\right]\right\} \tag{29}$$

It will be noted that these expressions are not multiple-valued across the dislocation cut. A reference to the stress equations (1) will indicate that the determined forms of the functions A(z) and B(z) for the logarithmic spiral case prevent any stress components from becoming multiple-valued. Therefore, all stress components across the dislocation cut should be continuous for the logarithmic spiral case. To keep with the convention of the method, however, equations (28) and (29) will still be referred to as the multiple-valued part of the stress.

III. APPLICATION TO A HOLE IN A LARGE PLATE

Single-valued Terms Constants

The final application of the equations of the previous section will be to a hole in a large plate. The hole has a logarithmic spiral dislocation extending from it into the plate. The single-valued term constants have to be determined for this case by using the procedure indicated in the previous subsection. That is, by substituting equations (25) and (28) into equation (26) and using

$$\sigma_r = \tau_{r\theta} = 0 \tag{5}$$

at the inner boundary r = a, and by substituting equations (25) and (29) into equation (26) and using condition (5) at the outer boundary $r = \infty$. In each case the vanishing of coefficients of like terms allows the determination of the single-valued term constants. Sine and cosine terms appear in both the real and imaginary parts of these equations, therefore, there result four equations at each boundary for each value of n. Even though in some cases some of these are dependent, the same number of independent equations as unknowns result so that all necessary constants can be determined. They are:

$$K_0 = \underset{n>0}{K_n} = 0 \quad , \quad K_{-1} \text{ immaterial}$$

$$K_{-2} = R_1 a^2\left(\frac{a^2}{2c^2} - 1\right) \quad , \quad \underset{n>2}{K_{-n}} = (-1)^n R_1 a^n \left(\frac{a}{c}\right)^n \left[\frac{1}{n} - \frac{c^2}{a^2(n-1)}\right]$$

$$L_1 = L_2 = L_{-2} = 0 \quad , \quad L_{-1} \text{ and } L_0 \text{ immaterial}$$

$$L_n = \underset{n>2}{L_{-n}} = 0$$

$$M_0 = -R_1 a^2 \left(1 + 2 \ln \frac{c}{a}\right), \quad M_{-1} = a^3 R_1 \left(\frac{c}{a} - \frac{a}{2c}\right)$$

$$M_{-2} = R_1 a^4 \left(\frac{2a^2}{3c^2} - 1\right), \quad \underset{n>2}{M_{-n}} = a^{n+2} (-1)^n R_1 \left(\frac{a}{c}\right)^n \left(\frac{n}{n+1} - \frac{c^2}{a^2}\right)$$

$$M_2 = 0, \quad \underset{n>2}{M_n} = 0, \quad M_1 \text{ immaterial}$$

$$N_0 = N_{-1} = N_2 = N_{-2} = \underset{n>2}{N_n} = \underset{n>2}{N_{-n}} = 0$$

N_1 immaterial

Circumferential Stress at Inner Boundary

The radial stress is zero at r = a according to condition (5), therefore, the only principal stress acting at this boundary is circumferential. The calculation of this stress will provide convenient correlation with the stress pattern obtained by photoelastic experiment. A basic equation from Wang (7) is

$$\sigma_r + \sigma_\theta = 4 \operatorname{Re} \phi_1'(z)$$

or since $\sigma_r = 0$ at r = a

$$\sigma_\theta = 4 \operatorname{Re} \phi_1'(z) \qquad (30)$$

The first of equations (15) and (20), expansions (1) and (3) of Appendix II, and the first of equations (24) with the single-valued part constants included, all substituted into equation (30) results in at r = a:

$$\frac{\sigma_\theta}{R_1} = 4\left\{\ln\frac{c}{a} + \frac{a}{c}\left(1-\frac{c^2}{a^2}\right)\cos\theta - \left(\frac{a}{c}\right)^2\left(1-\frac{c^2}{a^2}\right)\cos 2\theta + \left(1-\frac{c^2}{a^2}\right)\sum_{n=3}^{\infty}\left(\frac{a}{c}\right)^n(-1)^{n+1}\cos n\theta\right\} \tag{31}$$

Data calculated from this equation for a/c = 1/2 are summarized in Table I and are plotted on Curve 2. Thirteen terms were used in each individual series for these calculations. The stress at a given point on the inner boundary can be either tension or compression depending on the algebraic sign of the constant R_1. This sign is determined by the sign of the constant δ_2 that is included in R_1.

Maximum Shear Stress Along Cut

Another stress pattern of interest and one that can conveniently be correlated with photoelastic experiment is the maximum shear stress along the dislocation cut. A convenient form for calculating this stress is

$$\tau_{max} = \frac{\sigma_1 - \sigma_2}{2} = \sqrt{\left(\frac{\sigma_\theta - \sigma_r}{2}\right)^2 + \tau_{r\theta}^2} \tag{32}$$

TABLE I

CIRCUMFERENTIAL STRESS VALUES

θ°	σ_θ/R_1	MAX. PERCENT ERROR	θ°	σ_θ/R_1	MAX. PERCENT ERROR
0	-1.22772	0.06	180	14.77116	0.01
10	-1.21296	0.08	190	13.74324	0.17
20	-1.17300	0.12	200	11.27196	0.01
30	-1.10136	0.26	210	8.49192	0.18
40	-0.99528	0.13	220	6.07128	1.43
50	-0.84972	0.23	230	4.18332	0.39
60	-0.65616	0.44	240	2.82036	0.23
70	-0.40008	0.36	250	1.72920	0.86
80	-0.06756	7.30	260	0.95268	0.73
90	0.37308	0.19	270	0.37308	0.19
100	0.95268	0.73	280	-0.06756	7.30
110	1.72920	0.86	290	-0.40008	0.36
120	2.82036	0.23	300	-0.65616	0.44
130	4.18332	0.39	310	-0.84972	0.23
140	6.07128	1.43	320	-0.99528	0.13
150	8.49192	0.18	330	-1.10136	0.26
160	11.27196	0.01	340	-1.17300	0.12
170	13.74324	0.17	350	-1.21296	0.08
180	14.77116	0.01	360	-1.22772	0.06

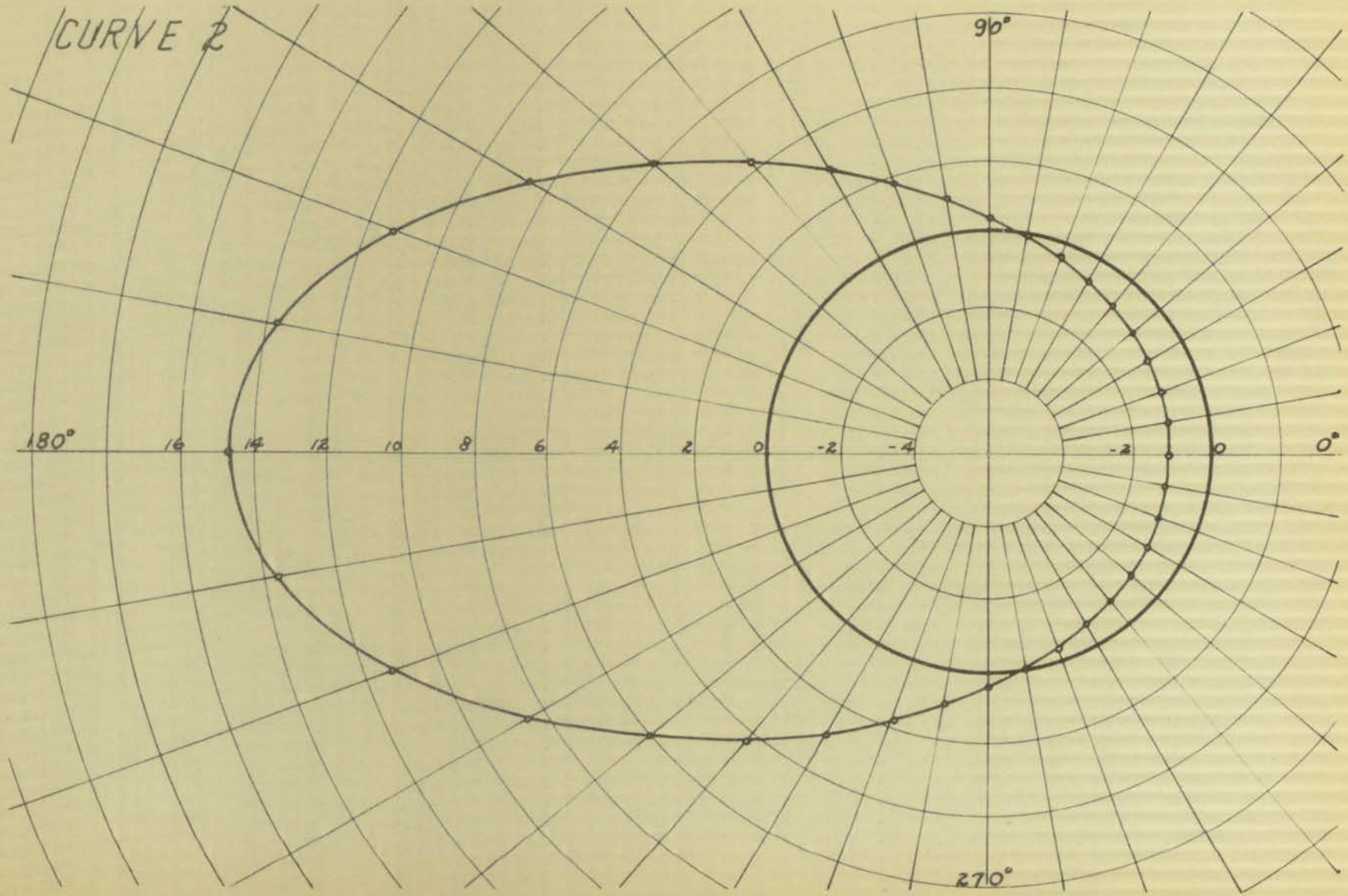
CURVE 2
90°
180°
16
14
12
10
8
6
4
2
0
-2
-4
-2
0
0°
270°

The individual components can be gotten from

$$\frac{\sigma_\theta - \sigma_r}{2} + i\tau_{r\theta} = \left[\bar{z}\,\phi_1''(z) + \phi_2''(z)\right]e^{2i\theta}$$

Substituting in the determined functions $\phi_1(z)$ and $\phi_2'(z)$, along with expansion (5) of Appendix II and the single-valued constants, results in

$$\frac{\sigma_\theta - \sigma_r}{2} = C_0 + C_1\cos\theta + \sum_2^\infty C_n \cos n\theta$$

where

$$C_0 = R_1\left[\left(\frac{a}{r}\right)^2\left(1+2\ln\frac{c}{a}\right)-1\right]$$

$$C_1 = R_1\left[\frac{r}{c} - 2\left(\frac{a}{r}\right)^3\left(\frac{c}{a} - \frac{a}{2c}\right)\right]$$

$$C_n = R_1\left\{\left(\frac{c^2}{r^2}-1\right)\sum_2^\infty (-1)^n\left(\frac{r}{c}\right)^n + \sum_2^\infty (-1)^n\left(\frac{a}{c}\right)^{2n}\left(\frac{c}{r}\right)^n\left[n\left(1+\frac{c^2}{r^2}-\frac{c^2}{a^2}-\frac{a^2}{r^2}\right)+\left(\frac{c^2}{r^2}-1\right)\right]\right\}$$

and

$$\tau_{r\theta} = C_1\sin\theta + \sum_2^\infty C_n \sin n\theta$$

where

$$C_1 = R_1\left[\left(\frac{r}{c}-\frac{2c}{r}\right) + 2\left(\frac{a}{r}\right)^3\left(\frac{c}{a}-\frac{a}{2c}\right)\right]$$

$$C_n = R_1\left\{\left(\frac{c^2}{r^2}-1\right)\sum_2^\infty (-1)^n\left(\frac{r}{c}\right)^n - \sum_2^\infty (-1)^n\left(\frac{a}{c}\right)^{2n}\left(\frac{c}{r}\right)^n\left[n\left(1+\frac{c^2}{r^2}-\frac{c^2}{a^2}-\frac{a^2}{r^2}\right)+\left(\frac{c^2}{r^2}-1\right)\right]\right\}$$

Substitution of these equations into equation (32) allows the calculation of maximum shear stress along the cut. Table II gives a summary of results of the calculation of stress components for a/c = 1/2. Curve 3 shows a plot of maximum shear stress variation with location along the dislocation cut.

TABLE II

STRESS VALUES ALONG CUT

ANGLE	NUMBER TERMS	$\frac{\sigma_\theta - \sigma_r}{2R_1}$	MAX. % ERROR	NUMBER TERMS	$\frac{\tau_{r\theta}}{R_1}$	MAX. % ERROR
140° 17' 7"	16	3.06676	0.05	∞	0.00000	0.00
150°	16	2.07733	0.70	16	2.43906	5.40
160°	22	0.75544	0.44	18	3.61445	0.70
170°	45	-0.07947	6.25	36	2.27117	1.57
175°	90	-0.28924	3.26	72	1.53921	3.61
180°	∞	0.59658	0.00	∞	0.00000	0.00

ANGLE	$\frac{\tau_{max}}{R_1}$
140° 17'7"	3.06676
150°	2.59890
160°	2.04576
170°	1.50912
175°	1.27392
180°	0.59658

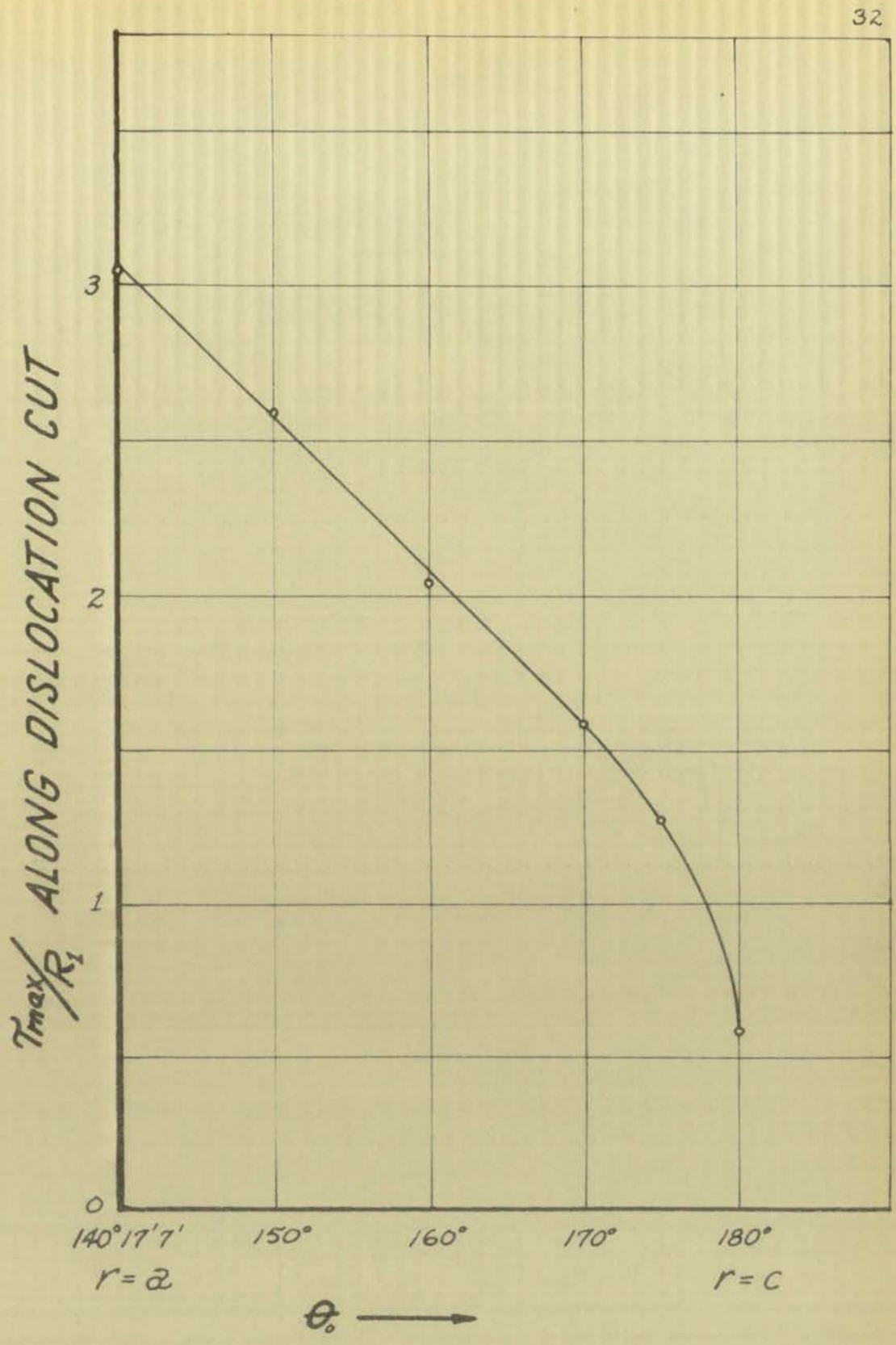
τ_{max}/R_1 ALONG DISLOCATION CUT
3
2
1
0
140°17'7'
150°
160°
170°
180°
r = a
r = c
θ_0

CURVE 3

IV. PHOTOELASTIC MATERIAL RESEARCH

There is no known experimental solution of a dislocation problem of the type discussed in the previous chapters of this paper. Before an experimental solution was attempted it was necessary to determine the approach to be used. The photoelastic technique was deemed feasible to study the logarithmic spiral dislocation at a hole in a large plate. A suitable photoelastic material as well as a model preparation procedure had to be determined. Essentially the problem was to cut a hole in a large piece of photoelastic material, then devise a method of causing a logarithmic spiral dislocation to extend from the hole to a point twice one radial distance from the center of the hole. The size specifications would then correspond to those of the analytical solution so that a correlation could be made.

Two methods of causing the dislocation were considered. The first will be referred to as the gluing method. It consists of cutting the dislocation into the material, drawing the dislocation edges back together with the relative displacement set, and gluing the edges together. Release of the edges after the glue had dried would cause a stress pattern that would correspond to an interference of material. This method would require a material that could be drawn easily, and also that could be glued with a suitable glue that would not induce stress upon drying. The second method will be referred to as the wedge method. It consists of cutting as narrow as possible a logarithmic curve into the material, then driving a suitably shaped wedge into the cut to provide the dislocation. This method would simulate a separation of material. Except for an inversion of the algebraic sign of all stresses, the result-

ing stress patterns would be identical for both methods of causing the dislocation. The adaptability of a given material to one of the two methods would determine which method is to be used. Accordingly, several materials were investigated. All photographs that appear in this paper were taken with a polaroid camera mounted on an 8-inch field polariscope.

CR 39 Plastic

The well known CR 39 photoelastic material was first investigated. It is a material of high photoelastic constant (about 90 psi-inch/fringe), but unfortunately it is quite rigid and brittle. The material can be sawed satisfactorily at high cutting speeds, and the sawed edges can be machined to a smooth finish on an end mill using a high cutting speed and a very slow feed. Two different glues were tried to determine the glue-induced stress properties. Neither Duco cement, nor Eastman 910 adhesive bond caused appreciable stress to be induced in this material. Figures 3 and 4 show the effects of these glues on CR 39. Figure 5 shows the glued blocks of Figure 4 acting as a single piece of material under stress. No significant stress relaxation with time was noted. Figures 6 through 9 show the transmission of stress across a surface of CR 39 glued with Eastman 910 adhesive bond. It will be noted that there is no appreciable stress relaxation with time.

These properties of CR 39 seemingly adapted it very well to be used as a material for the dislocation problem. A model was prepared to use the wedge dislocation method. This material is much too rigid to have allowed the gluing method to be used. So that a very narrow smooth dislocation cut could be attained, the 30 x 30 x 1/4 inch slab of material used was cut horizontally through to the hole and along the intended

dislocation cut. It was then machined along these surfaces and glued back together except along the dislocation cut. The two pieces matched together to form a large plate with a three inch diameter hole and a thin logarithmic spiral cut extending to three inches from the center of the hole. Unfortunately this material was so brittle that it cracked when an aluminum dislocation wedge was inserted into the cut. As a result CR 39 was not further considered a suitable material for the dislocation problem.

Hysol 8705 Plastic

Hysol 8705 is a very flexible, low modulus photoelastic material. It has a photoelastic constant of about three psi-inch/fringe. The low modulus of this material makes it very suitable to sustain easy displacement, therefore, it is well suited in this respect to be used as a dislocation model. Hysol can be cut very readily using a band saw with a fine tooth blade at high cutting speeds and very slow feed. It cannot be machined on a tool machine very well, but can be smoothed satisfactorily on an emery wheel or a belt sander at high speed. Water can be used as a lubricant for this abrasive process. Care must be exercised to prevent the hysol from becoming overheated for it will melt easily. The material has comparatively poor gluing properties when glued with Duco cement. Figure 10 shows high stress induced from the use of this glue. Eastman 910 adhesive bond, however, produced good results with this material. Figures 11 and 12 show glue induced stress from the use of this bond. Figure 12 seemed to show a very good bond, however, the same piece of material under stress, shown in Figure 13, did not act

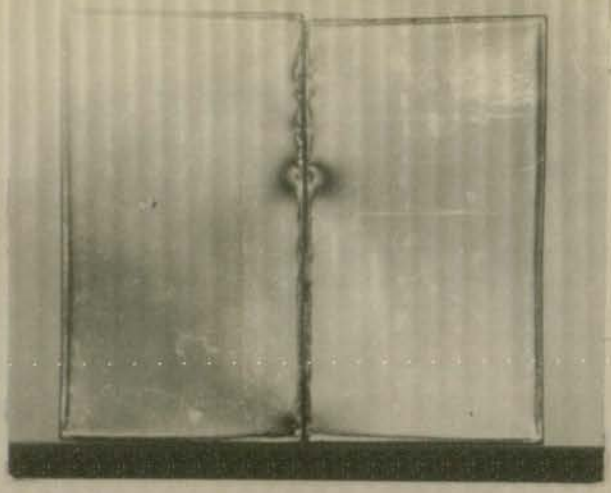

Figure 3 CR 39 and Duco Cement
44 Hours After Gluing

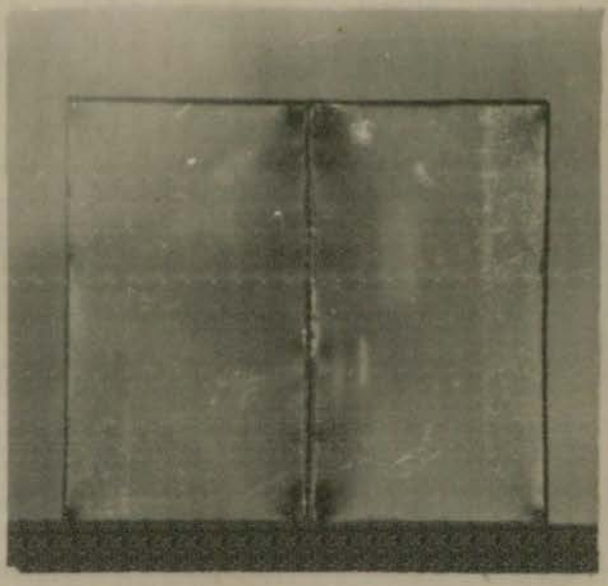

Figure 4 CR 39
and Eastman 910
1/2 Hour After Gluing

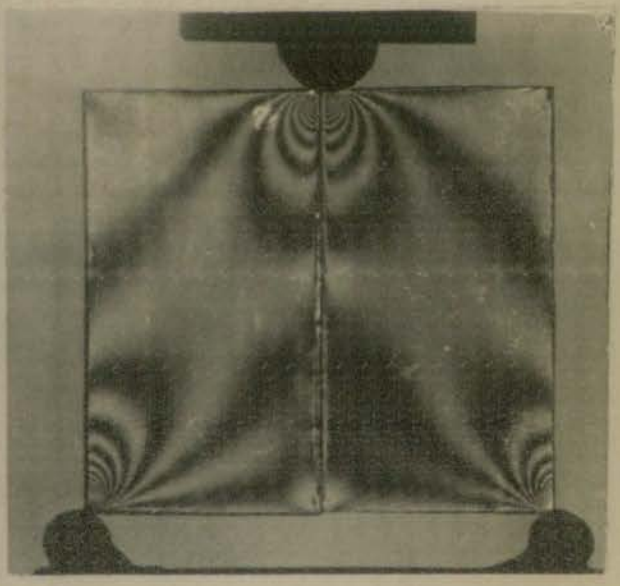

Figure 5 CR 39
Acting As One Piece

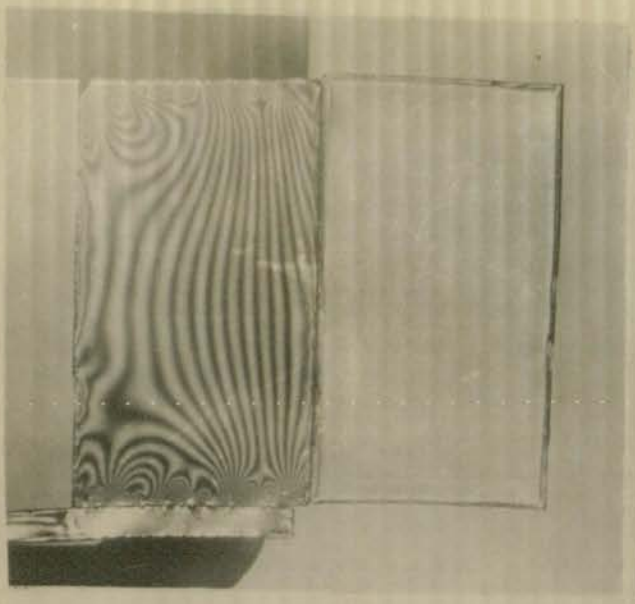

Figure 6 CR 39
Clamped and Glued

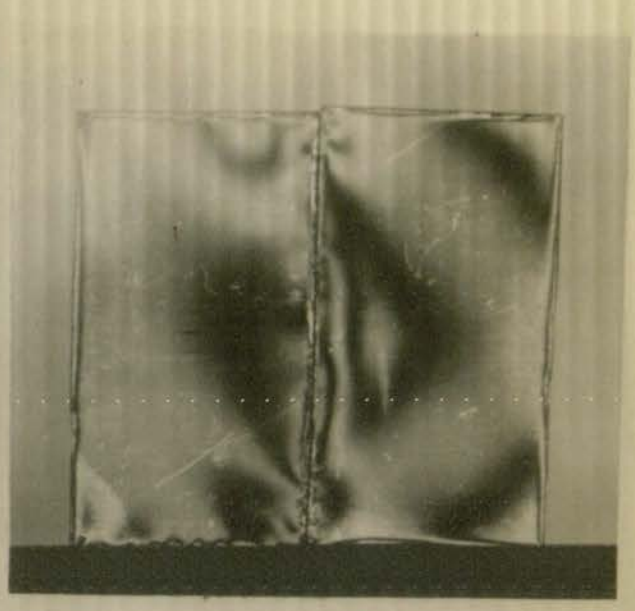

Figure 7 CR 39
At Release

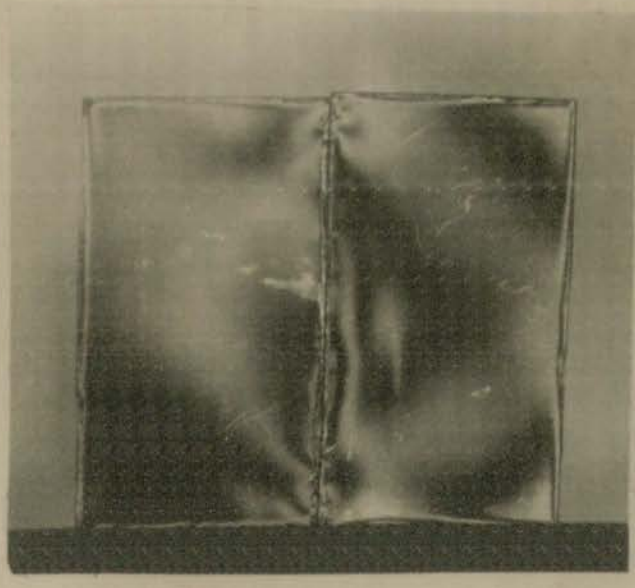

Figure 8 CR 39
30 Minutes After Release

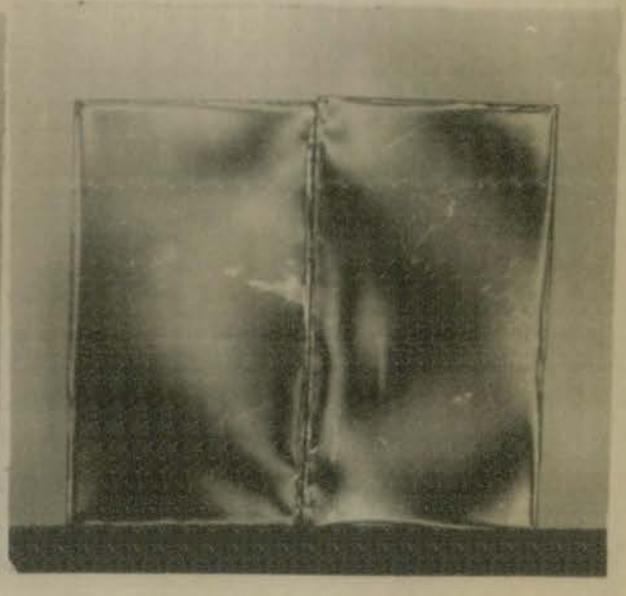

Figure 9 CR 39
One Hour After Release

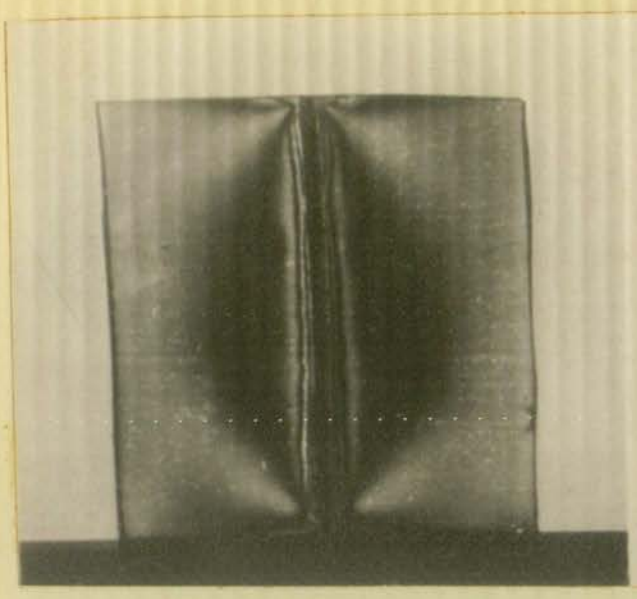

Figure 10 Hysol 8705
and Duco Cement
One Hour After Gluing

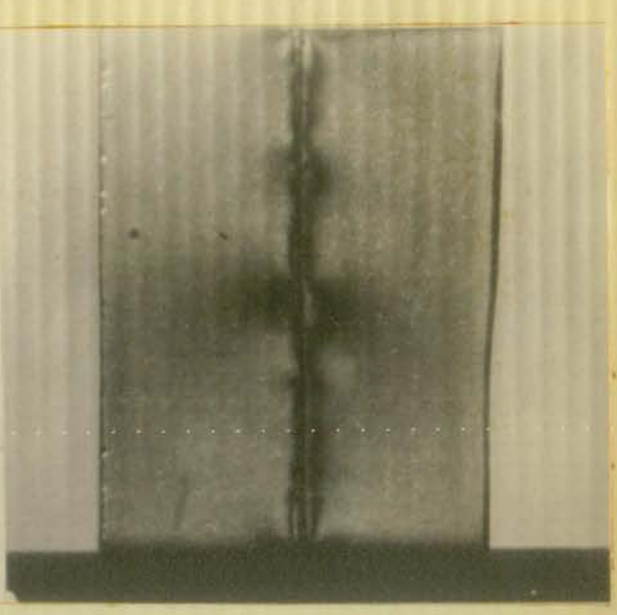

Figure 11 Hysol 8705
and Eastman 910
30 Minutes After Gluing

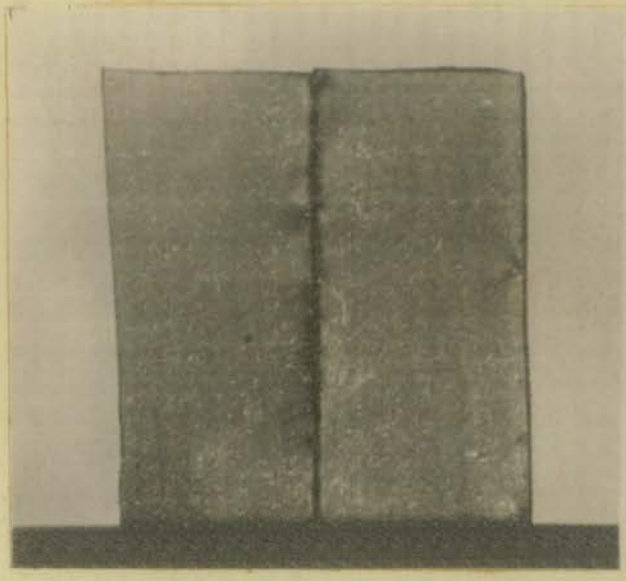

Figure 12 Hysol 8705
and Eastman 910
30 Minutes After Gluing

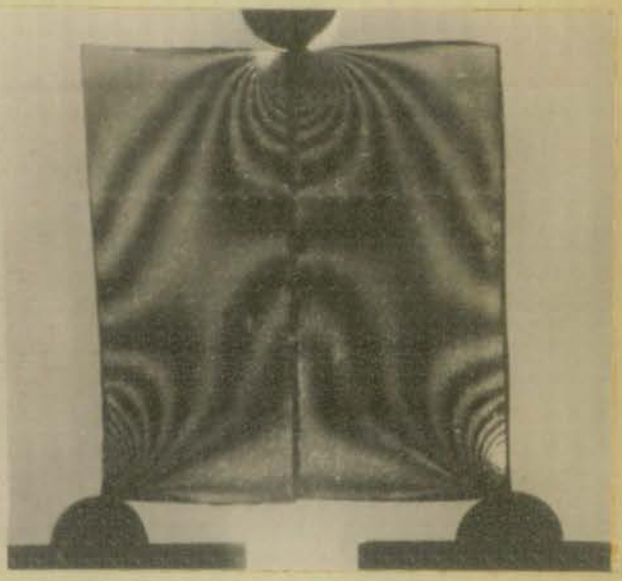

Figure 13 Hysol 8705
and Eastman 910
Acting Almost As One Piece

as one piece. Some shift in fringes across the glued surface can be noted. The results of these tests indicated that the wedge method of dislocation would be the most suitable to make a dislocation model of this material.

Adiprene Plastic

Adiprene is a photoelastic material that was cast locally in the plastics shop. Appendix III gives the casting specifications and procedure for this material. Physically adiprene is very much like Hysol 8705 except that it is somewhat more transparent. Its low modulus is about the same as that of hysol, and its cutting and smoothing properties are about the same. The model fabrication procedure then would be the same as that of hysol. The photoelastic constant for adiprene was determined to be about four psi-inch/fringe. A simply supported beam with a central concentrated load was used for this determination. Curve 4 shows the linearity of load with stress fringes up to 20 fringes for adiprene. It can be seen that the material is essentially linear and no hysteresis is involved, for the curve holds for both loading and unloading. The linearity test was also conducted using a centrally loaded, simply supported beam. No significant stress relaxation with time was noted. Gluing properties of adiprene are about the same as for hysol, so that it also is not suitable for the gluing method of dislocation. It is very well suited to the wedge method of dislocation. The immediate availability of a large piece of this material resulted in its being used for the final dislocation model. Hysol 8705 could also have been used since the two materials are nearly alike.

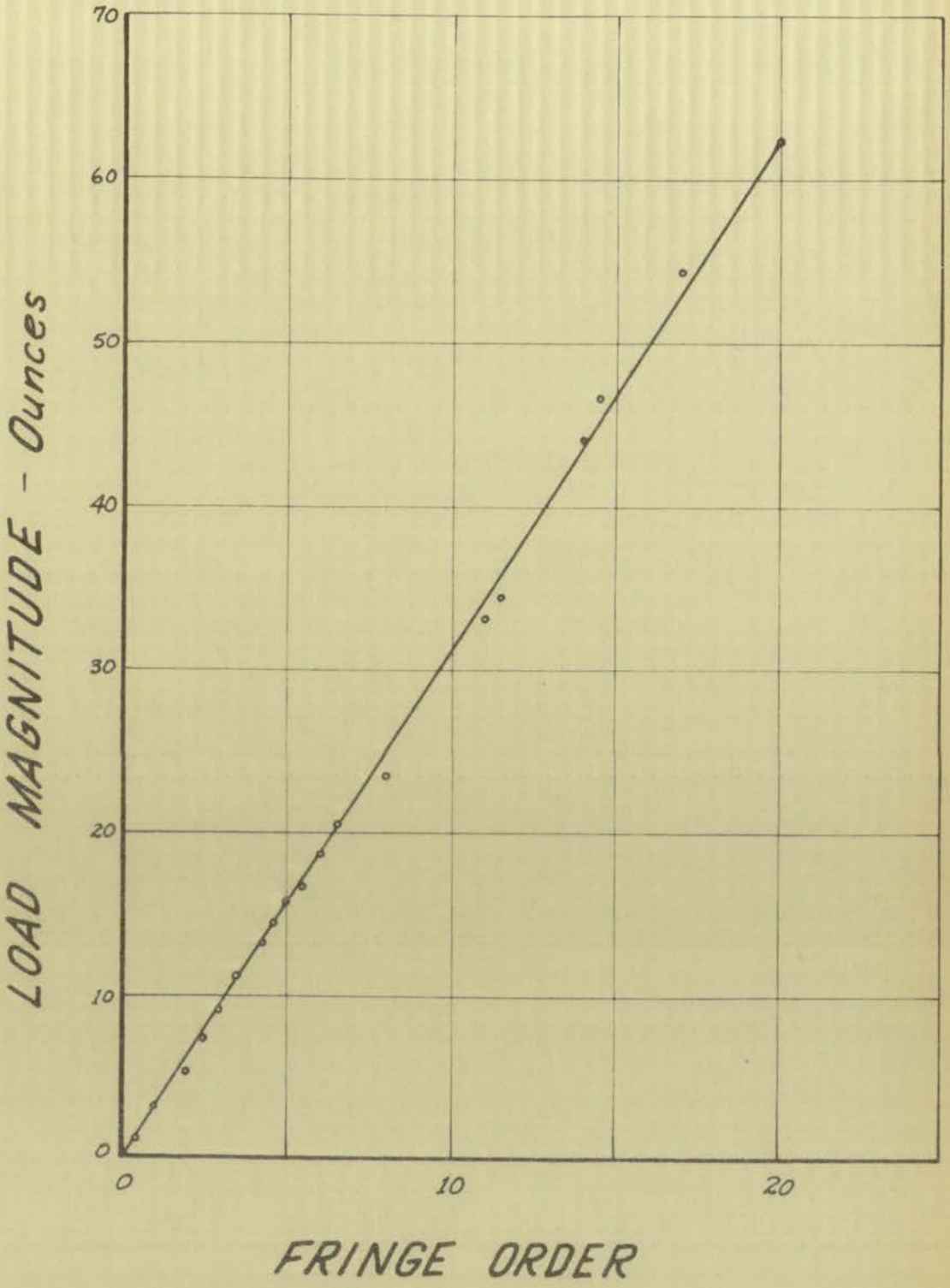
LOAD MAGNITUDE - Ounces
70
60
50
40
30
20
10
0
0
10
20
FRINGE ORDER

CURVE 4

V. EXPERIMENTAL SOLUTION

As a result of the material research of the previous chapter, the adiprene plastic was used for the photoelastic model for the experimental solution of the logarithmic spiral dislocation in a large plate. The wedge method was used to provide the dislocation. The following chapter relates procedures used and the results of that solution.

Model Preparation

A 19-inch diameter, 1/2-inch thick, round slab of adiprene plastic was used as the basic material for the dislocation model. The solution sought was the stress pattern caused by a logarithmic spiral dislocation near a hole in a large plate. The 19-inch diameter slab was the largest piece of the material available. The logarithmic spiral dislocation had to be made to extend to twice the radial distance from the center of the hole so that a correlation with the analytical solution could be made. A three-inch diameter hole was considered feasible. This size hole was large enough to allow measuring displacements with reasonable accuracy, and was not too large in relation to the size of the slab so that a large plate could be assumed.

A three inch diameter circle and a logarithmic spiral with $\beta = 45^{\circ}$ were first scribed in ink at the intended location near the center of the slab of plastic. Various guide lines were also scribed on the material. The logarithmic spiral was first drawn on polar coordinate paper and traced onto the plastic. It was drawn to extend from the hole boundary at $r = 1.5$ inches, θ, about 140°, to $r = 3.0$ inches (two radii), and $\theta = 180^{\circ}$. This corresponded to the analytical problem.

The hole was cut into the plastic first. A small hole was punched within the circle so that a band saw blade could be inserted. It was necessary to part the blade, of course. Upon rejoining the blade, the hole was then cut along the circle scribed on the material. A fine tooth blade at high cutting speed and very slow feed was used. About 1/16-inch of material was left inside the hole to allow for smoothing on the emery wheel. The saw blade had to be broken to be removed. Smoothing of the inside of the hole surface was accomplished on a 2 3/4-inch diameter emery wheel running at high speed. Water was used as a lubricant. The smoothing operation was kept even by moving the plastic slab in an eccentric circular path in the plane of the emery wheel rotation. The point of contact of the wheel with the inside surface of the hole would then move around the inside of the hole in a constant direction. Care had to be exercised to prevent overheating and melting the plastic. It was also kept in mind that overheating the plastic might change its photoelastic properties in the immediate vicinity of the hole. This would have been very undesirable, of course.

The logarithmic spiral was cut into the material by inserting a band saw blade into the hole, rejoining the blade tips, and sawing in the logarithmic spiral curve. Again a fine tooth blade at high cutting speed and slow feed was used. The thinest blade available was used to provide as narrow a cut as possible. A 3/8-inch wide blade was used to allow the scribed curve to be followed easily. The thinest blade available still made a cut of about 0.05 inches width. This was considered thin enough for the length of cut and size of hole used. The inside surfaces of the cut were smoothed with emery paper. Care had to be exercised to

prevent removing too much material so that the order of width remained unchanged.

The wedge was fabricated also from adiprene plastic. However, the piece from which the wedge was made had been cured by a different process than the large slab of the model. The wedge material was somewhat more rigid. Nevertheless the wedge material was still very flexible in bending so that the wedge very readily conformed to the curved shape of the opened dislocation cut in the large slab. No loss of contact in model material surface and wedge material surface could occur as a result. The wedge was then fairly rigid against normal pressure, but was very flexible in bending. The wedge was made to be linear in normal thickness along the length from its tip. This would approximately conform to the normal dislocation required by the analytical solution. The wedge itself would allow no control of the tangentical dislocation along the cut. The actual wedge fabrication was accomplished by scribing the wedge shape on the plastic, cutting it out with the band saw, and smoothing the surfaces with the emery wheel and emery paper.

Stress Solution

To form the stress field for viewing in the polariscope the wedge was simply inserted snugly into the logarithmic spiral cut extending from the hole in the slab of adiprene plastic. The plastic slab was then clamped onto a support frame to help keep it in a vertical plane. The low modulus material had a tendency to buckle otherwise. Figure 14 shows the stress pattern as viewed in the polariscope. Proportional distances can be measured on the photograph by keeping in mind that the undistorted

hole diameter is three inches. This photograph was made by splicing together nine separate photographs of the stress field. Any dark area near the outer border of the photograph is not part of the dislocation stress pattern. The dislocation wedge is inserted entirely to the end of the cut at 180°. The dark line appearing between 170° and 175° on the wedge must not be mistaken to be the tip of the wedge. This line was caused by a slip of the wedge on the emery wheel during the fabrication.

It is obvious that the stress pattern as a whole is symmetrical about the horizontal axis. The actual normal and tangential dislocation obtained along the cut in the model was carefully measured on the photograph. The radial guide lines were used for the measurements. When making these measurements it must be recalled that the initial width of the non-dislocated cut was 0.05 inch. Curve 5 shows a comparison of the experimental normal and tangential dislocations along the cut with the dislocations required by the analytical solution. It can be seen that the dislocations somewhat coincide. The comparison is very good considering that no great effort was exerted to control the dislocation variation tangent to the cut. As a result, the experimental stress pattern should be nearly the same as that predicted by the analytical solution if that solution is valid. Curve 6 shows a plot of the experimental circumferential stress around the edge of the hole. A comparison of this plot with the analytical plot on Curve 2 shows that the two are very nearly alike. Curve 7 shows some experimental points of the maximum shear stress along the cut plotted onto the analytical solution for this stress. It can be seen that the experimental points fall well along

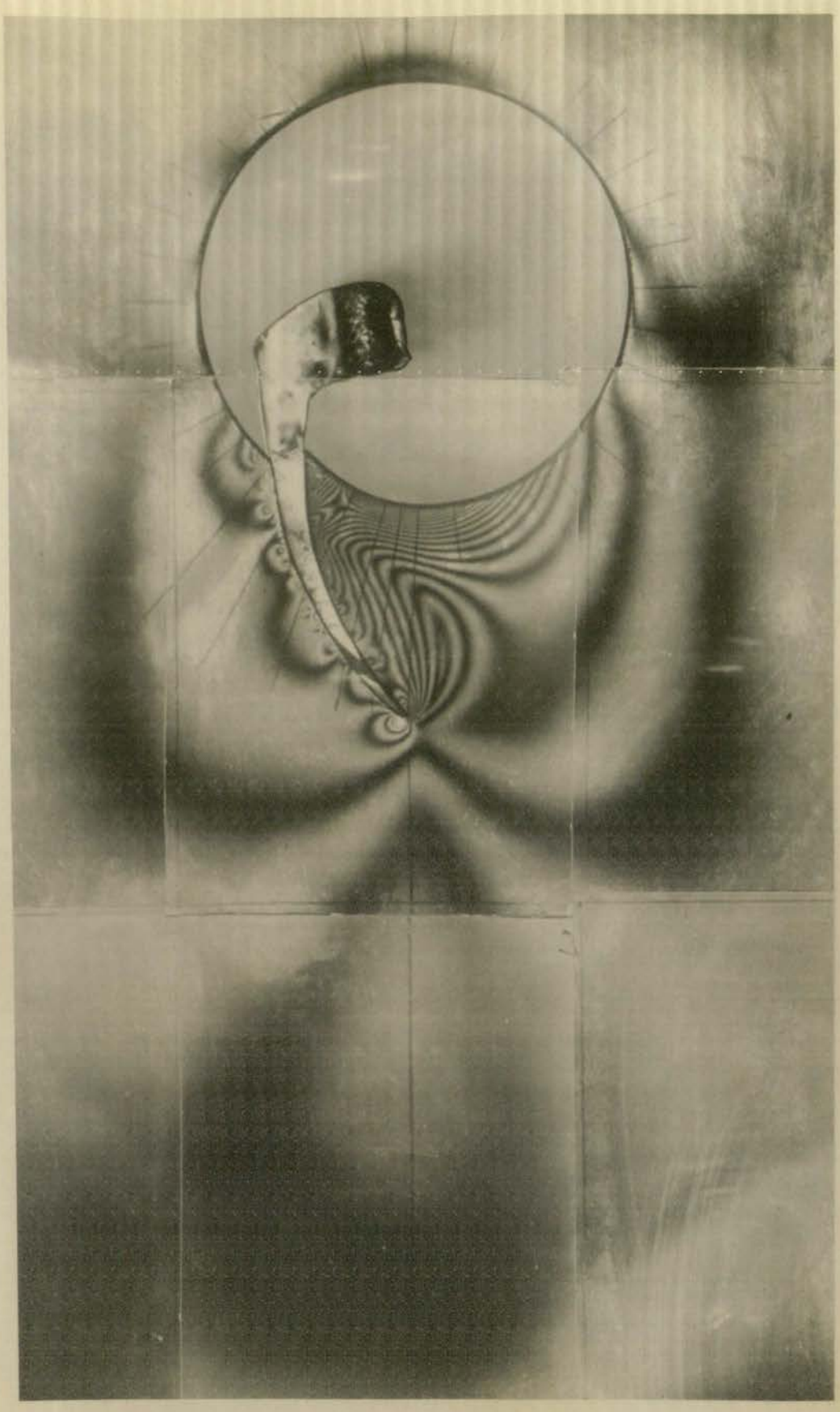

Figure 14

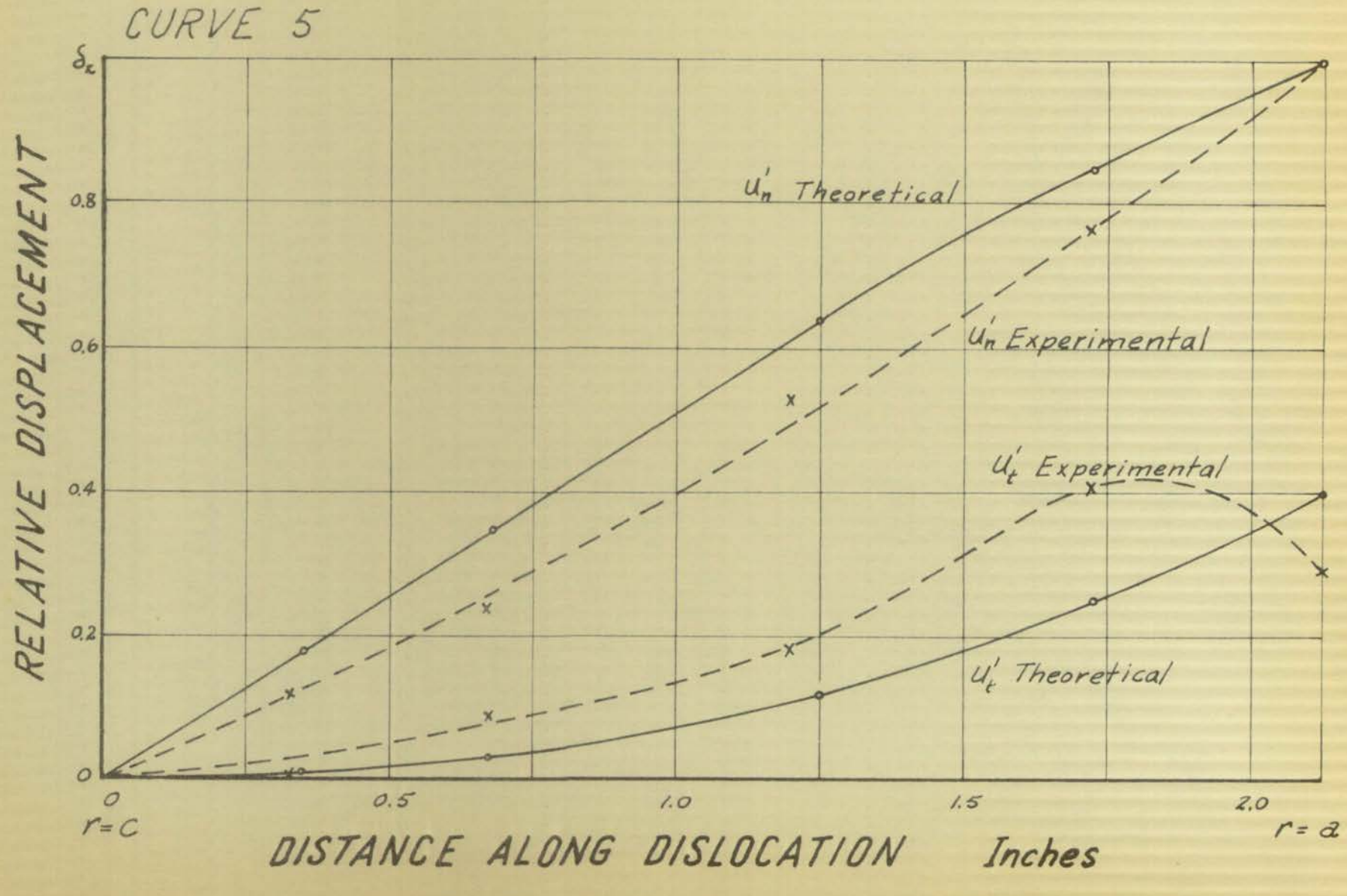
CURVE 5
δ_c
0.8
0.6
0.4
0.2
0
RELATIVE DISPLACEMENT
u'_n Theoretical
u'_n Experimental
u'_t Experimental
u'_t Theoretical
0
0.5
1.0
1.5
2.0
r=C
r=a
DISTANCE ALONG DISLOCATION Inches

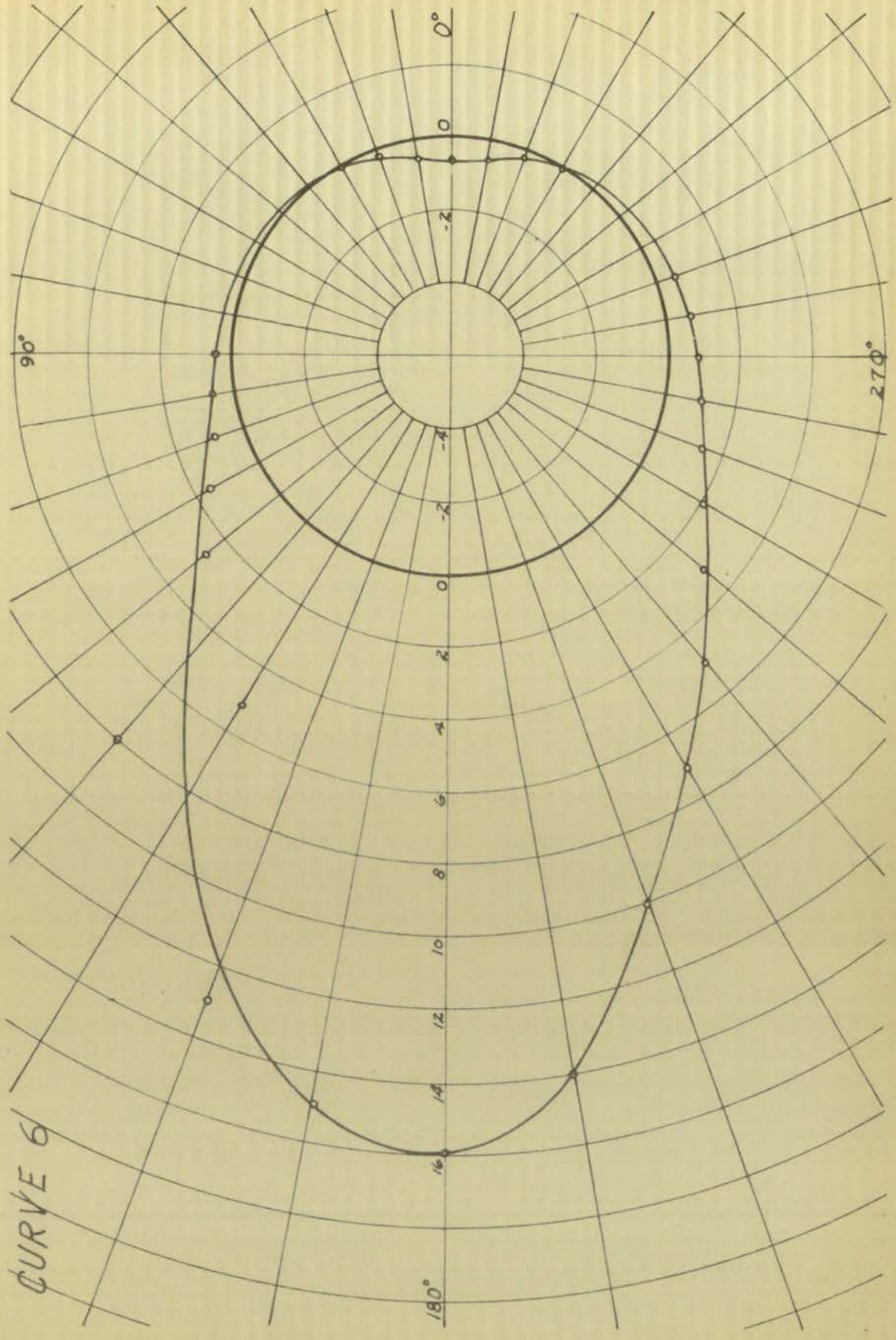

CURVE 6

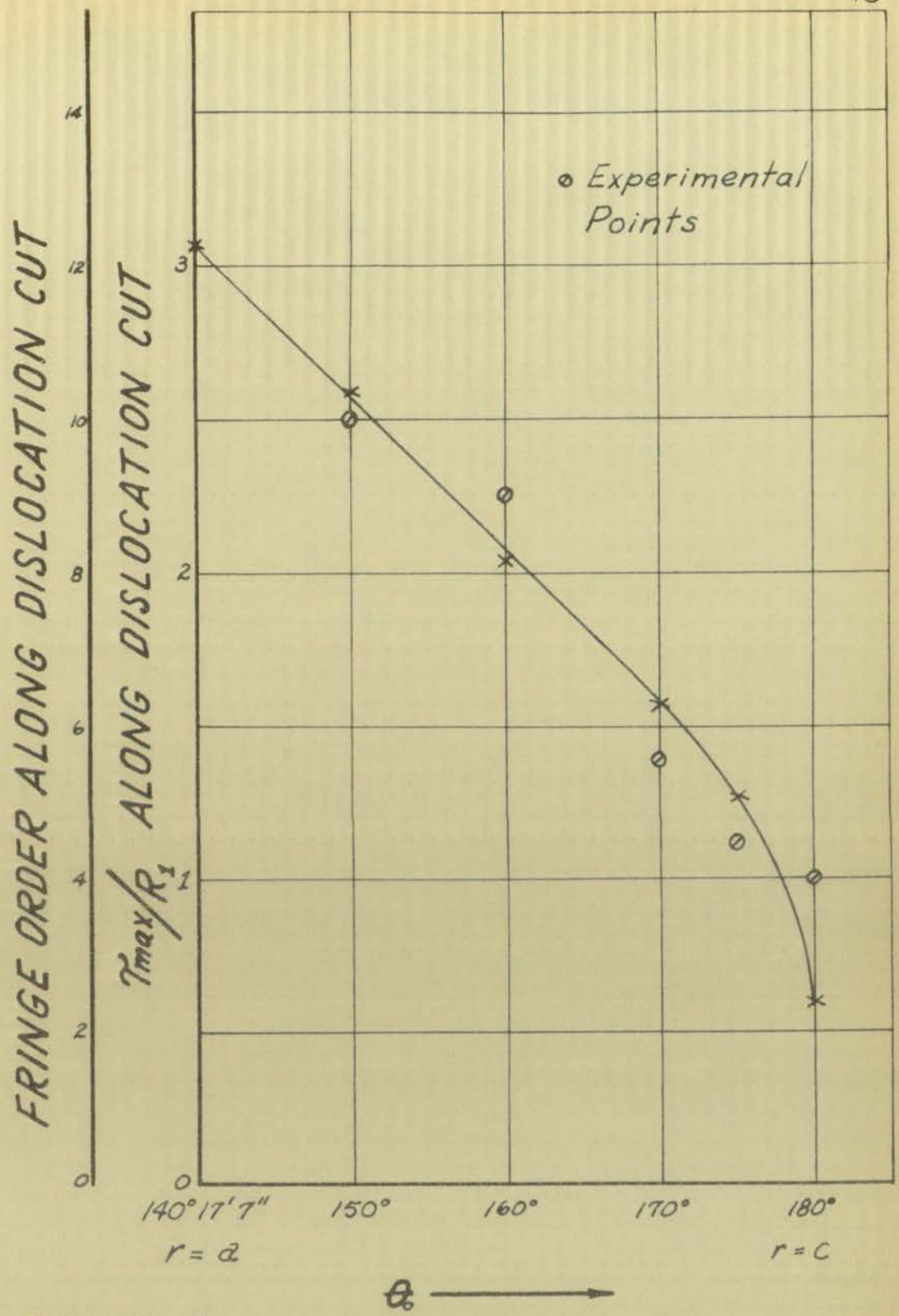
FRINGE ORDER ALONG DISLOCATION CUT
τ_{max}/R_1 ALONG DISLOCATION CUT
Experimental Points
0
2
4
6
8
10
12
14
0
1
2
3
140° 17' 7"
150°
160°
170°
180°
r = a
r = c
θ

CURVE 7

the analytical recults. These experimental values of maximum shear stress along the cut were taken only from the lower side of the dislocation in the material. The fringe order at the terminus was arbitrarily taken to coincide nearly with the stress value at that point of the analytical curve. The relative position of other experimental stress points along the dislocation cut could then be plotted. A difference in slope could be expected. The experimental stress on the upper side of the dislocation does not conform with the analytical prediction very well. The stress across the cut does not appear to be continuous as was predicted, and the pattern on the upper surface of the cut is locally distorted because of small irregularities in the sawed dislocation cut. Any further attempt at removing these irregularities with emery paper would have caused error regardless, because the width of the cut would have become too large. The nonconforming of the stress pattern on the upper side of the cut and stress discontinuity across the cut could also have resulted from experimental absolute displacements along the upper side of the cut not being exactly the same as those of the analytical solution. The upper side of the cut is along a stiffer part of the model, therefore, it probably did not displace as the analytical solution would require. A controlled absolute displacement as well as controlled dislocation along the cut would provide a better correlation in this portion of the stress pattern.

VI. CONCLUSION

The overall comparison of the experimental and analytical results of the stresses considered is very good. The experimental results of this paper, therefore, support the results of the dislocation theory applied to the logarithmic spiral in a large plate. As was indicated earlier, a still better correlation of experimental and analytical results could be obtained by devising a method of controlling both displacements and the dislocation along the cut in the experimental model. The displacements and dislocation could then be made to correspond more closely to those required by the analytical solution. The calculation of displacements from the analytical solution would involve computations with infinite series as did the stresses that were calculated in this paper. Localized stress distortion along the cut could be avoided in future models by using a still thinner and narrower band saw blade to cut in the dislocation curve. Also a jig should be used on the saw so that the blade could be made to follow the intended cut line more smoothly.

The symmetry of the circumferential stress at the hole would seem to imply that as the logarithmic spiral dislocation would progress further into the material, the stress pattern would rotate to remain symmetrical about the axis that passes through the terminus of the cut and the center of the hole. The terminus area would then be continuously an area of comparatively low stress. This implication, along with the pattern for maximum shear stress along the cut, does not seem feasible for the practical case of a Lueders' band in a thick-walled cylinder. Except for what is judged to be slight localized stress concentration around

the terminus in the experimental solution, both solutions indicate that stress at the terminus is lower than that indicated at the opening of the cut. The Lueders' band would necessarily have stress concentration at its terminus if the band is to progress into the material as internal pressure is increased. Therefore, the logarithmic spiral dislocation problem with the logarithmic form of multiple-valued function and its resulting unique dislocation relation may not be a very good approximation to the Lueders' band problem after all. More knowledge of the dislocation relation along a Lueders' band would be necessary to make this decision.

A physical interpretation of the experimental method of dislocation is possible. The wedge method directly simulates the result of the formation of a Lueders' band of plastic material in a thick-walled cylinder under high internal pressure. Upon release of internal pressure, the elastic material of the cylinder tends to relax to the undisplaced condition. The plastic material along the Lueders' band does not, however, and it effectively forms a wedge causing compression in the elastic region. A separation of elastic material has resulted.

A most interesting result of the solution of the logarithmic spiral problem is that all stress components remained continuous across the dislocation cut. Volterra's dislocation theory, summarized in reference (6), indicated that to have all stresses remain continuous in a region that has a dislocation it was necessary to have the dislocation connect both boundaries of a doubly-connected region, and the dislocation relation along the cut had to be constant. For the logarithmic spiral problem in this paper the dislocation cut did not connect both boundaries

of the doubly-connected region, and the dislocation was specified to be elastic along the cut, not constant. Complete stress continuity still resulted even though it was not required by elastic dislocation theory. Apparently the logarithmic spiral problem incorporating the $\ln \frac{z + c}{z}$ form of multiple-valued function is a special case of the elastic dislocation theory, and it indicates that the Volterra dislocation theory is not completely valid.

BIBLIOGRAPHY

1. Ju, F. D., "On the Airy Stress Functions of Plane Dislocation Problems", Journal of Applied Mechanics, Paper No. 60-APM-14, June 1960

2. Knopp, K., Theory and Application of Infinite Series, Hafner Publishing Co., New York, N. Y., 1947

3. Lee, G. H., An Introduction to Experimental Stress Analysis, John Wiley and Sons Inc., New York, N. Y., 1950

4. Mann, E. H., "An Elastic Theory of Dislocations", Proceedings of the Royal Society, Series A, Vol. 199, 1949

5. Sokolnikoff, I. S. and Redheffer, R. M., Mathematics of Physics and Modern Engineering, McGraw-Hill Book Co., New York, N. Y., 1958

6. Stippes, N. and Ju, F. D., "Some Plane Dislocation Problems", Theoretical and Applied Mechanics Report No. 123, University of Illinois, 1957

7. Wang, C. T., Applied Elasticity, McGraw-Hill Book Co., New York, N. Y., 1953

APPENDIX I

Proof That a Function Linear Along a Logarithmic Spiral is Linear in r_o

The equation of the logarithmic spiral passing through (-c, 0) is

$$\theta_o = \pi + \tan\beta \ln r_o/c$$

or

$$r_o = c\, e^{\left(\frac{\theta_o - \pi}{\tan\beta}\right)}$$

The arc distance along the curve is given by

$$S = \int_{\rho_1}^{\rho_2} \left[\rho^2 \left(\frac{d\theta}{d\rho}\right)^2 + 1 \right]^{\frac{1}{2}} d\rho$$

Substituting the above into this relation and integrating between the limits $\rho = c$ and $\rho = r_o$ there results

$$S = (1 + \tan^2\beta)^{\frac{1}{2}} (c - r_o)$$

For $\beta = 45^\circ$ this becomes

$$S = \sqrt{2}\,(c - r_o)$$

APPENDIX II

Expansions of Functions into Trigonometric Forms

1. $\ln \frac{z+c}{z}$ for $|z| < c$

$$\ln \frac{z+c}{z} = \ln\left(1+\frac{z}{c}\right) - \ln \frac{z}{c} - \int \frac{d\left(\frac{z}{c}\right)}{1+\frac{z}{c}} - \ln \frac{z}{c}$$

$$= \int \left[1 - \left(\frac{z}{c}\right) + \left(\frac{z}{c}\right)^2 - \cdots\cdots\right] d\left(\frac{z}{c}\right) - \ln \frac{z}{c}$$

$$= \sum_1^\infty \frac{(-1)^{n+1}}{n}\left(\frac{z}{c}\right)^n - \ln\left(\frac{r}{c}\right) - i\theta = \ln \frac{c}{r}$$

$$+ \sum_1^\infty \frac{(-1)^{n+1}}{n}\left(\frac{r}{c}\right)^n \cos n\theta + i\left[-\theta + \sum_1^\infty \frac{(-1)^{n+1}}{n}\left(\frac{r}{c}\right)^n \sin n\theta\right]$$

Since only the real part of this equation is necessary in equation (27), it is not necessary to expand further the $-\theta$ term into a Fourier series.

2. $\ln \frac{z+c}{z}$ for $|z| > c$

$$\ln \frac{z+c}{z} = \ln\left(1+\frac{c}{z}\right) = \int \frac{d\left(\frac{c}{z}\right)}{1+\left(\frac{c}{z}\right)} = \int \left[1 - \left(\frac{c}{z}\right) + \left(\frac{c}{z}\right)^2 - \cdots\right] d\left(\frac{c}{z}\right)$$

$$= \sum_1^\infty \frac{1}{n}\left(\frac{c}{z}\right)^n (-1)^{n+1} = \sum_1^\infty \frac{(-1)^{n+1}}{n}\left(\frac{c}{r}\right)^n e^{-in\theta}$$

$$= \sum_1^\infty \frac{(-1)^{n+1}}{n}\left(\frac{c}{r}\right)^n \cos n\theta + i \sum_1^\infty \frac{(-1)^n}{n}\left(\frac{c}{r}\right)^n \sin n\theta$$

3. $-\frac{c}{z}$ for $|z|<c$ and $|z|>c$

$$-\frac{c}{z} = -\frac{c}{r}e^{-i\theta} = -\frac{c}{r}(\cos\theta - i\sin\theta)$$

4. $\frac{1-e^{2i\theta}}{z(z+c)}$ for $|z|>c$

By partial fractions

$$\frac{1-e^{2i\theta}}{z(z+c)} = \frac{1}{cz} - \frac{e^{2i\theta}}{cz} + \frac{e^{2i\theta}-1}{c(z+c)}$$

Expanding the last term separately by long division

$$\frac{e^{2i\theta}-1}{c(z+c)} = -\frac{1}{rc}\left[\frac{1-e^{2i\theta}}{e^{i\theta}+c/r}\right] = -e^{i\theta} + \frac{c}{r} + \sum_{1}^{\infty}(-1)^{n-1}\left(1-\frac{c^2}{r^2}\right)\left(\frac{c}{r}\right)^{n-1}e^{-in\theta}$$

Combining the trigonometric forms of the three terms and grouping

$$\frac{1-e^{2i\theta}}{z(z+c)} = \frac{c}{r^3}\cos\theta - \frac{1}{r^2} + \left(\frac{1}{c^2}-\frac{1}{r^2}\right)\sum_{2}^{\infty}(-1)^n\left(\frac{c}{r}\right)^n\cos n\theta$$

$$-i\left[\frac{c}{r^3}\sin\theta + \left(\frac{1}{c^2}-\frac{1}{r^2}\right)\sum_{2}^{\infty}(-1)^n\left(\frac{c}{r}\right)^n\sin n\theta\right]$$

5. $\frac{1-e^{2i\theta}}{z(z+c)}$ for $|z|<c$

By partial fractions

$$\frac{1-e^{2i\theta}}{z(z+c)} = \frac{1}{cz} - \frac{e^{2i\theta}}{cz} + \frac{e^{2i\theta}-1}{c(z+c)}$$

Expanding the last term separately by long division

$$\frac{e^{2i\theta}-1}{c(z+c)} = -\frac{1}{rc}\left[\frac{1-e^{2i\theta}}{c/r+e^{i\theta}}\right] = -\frac{1}{c^2}+\frac{e^{i\theta}}{rc}+\left(\frac{1}{r^2}-\frac{1}{c^2}\right)\sum_{1}^{\infty}(-1)^n\left(\frac{r}{c}\right)^n e^{in\theta}$$

Combining the trigonometric forms of the three terms and grouping

$$\frac{1-e^{2i\theta}}{z(z+c)} = \frac{r}{c^3}\cos\theta-\frac{1}{c^2}+\left(\frac{1}{r^2}-\frac{1}{c^2}\right)\sum_{2}^{\infty}(-1)^n\left(\frac{r}{c}\right)^n\cos n\theta$$

$$+i\left[\left(\frac{r}{c^3}-\frac{2}{rc}\right)\sin\theta+\left(\frac{1}{r^2}-\frac{1}{c^2}\right)\sum_{2}^{\infty}(-1)^n\left(\frac{r}{c}\right)^n\sin n\theta\right]$$

APPENDIX III

Casting Specifications of Adiprene Plastic

Ingredients

100 Parts Adiprene L-100 (Basic Material)

8 Parts Trimethylolpropane (TMP) Curing Agent

Curing Process

Cure for 22 hours at 100° - 105° Centigrade

IMPORTANT!

Special care should be taken to prevent loss or damage of this volume. If lost or damaged, it must be paid for at the current rate of typing.

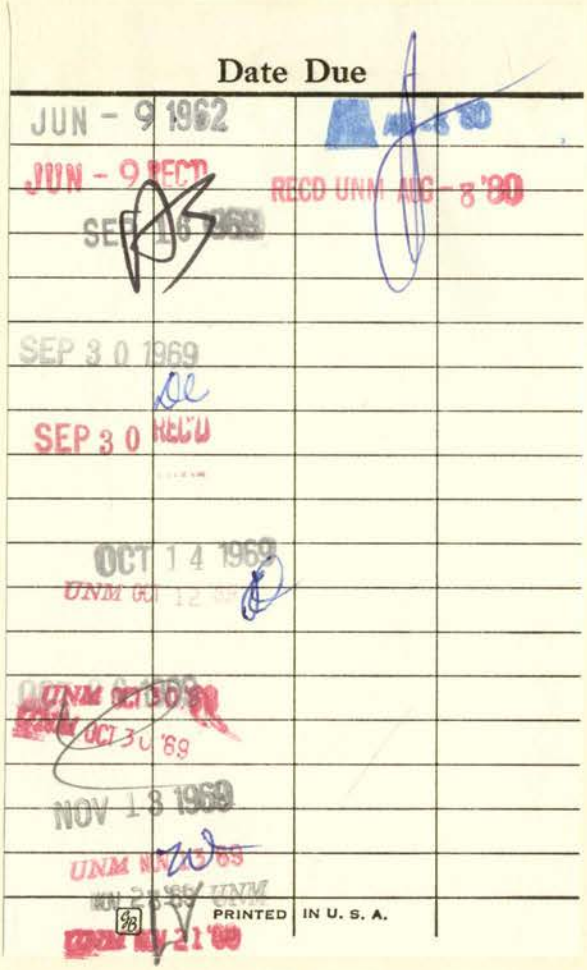

Date Due

JUN - 9 1962

JUN - 9 RECD

SEP 1 6 1969

SEP 3 0 1969

SEP 3 0 RECD

OCT 1 4 1969

UNM OCT 12

UNM OCT 30 '69

OCT 30 '69

NOV 1 8 1969

UNM NOV 18 '69

UNM

NOV 21 '69

PRINTED IN U. S. A.

RECD UNM AUG - 8 '80